IEEE Access
Multidisciplinary ⋮ Rapid Review ⋮ Open Access Journal

Received August 13, 2021, accepted August 29, 2021, date of publication September 6, 2021, date of current version September 14, 2021.

Digital Object Identifier 10.1109/ACCESS.2021.3110503

Coverage Performance of the Terrestrial-UAV HetNet Utilizing Licensed and Unlicensed Spectrum Bands

YIFAN JIANG[1], ZESONG FEI[1], (Senior Member, IEEE), JING GUO[1], AND QIMEI CUI[2], (Senior Member, IEEE)
[1]School of Information and Electronics, Beijing Institute of Technology, Beijing 100081, China
[2]National Engineering Laboratory for Mobile Network Technologies, Beijing University of Posts and Telecommunications, Beijing 100876, China

Corresponding author: Jing Guo (jingguo@bit.edu.cn)

This work was supported in part by Beijing Natural Science Foundation under Grant L182038, in part by National Natural Science Foundation of China under Grant 62001029, in part by Ericsson, and in part by Young Talents Supporting Project of China Association for Science and Technology.

ABSTRACT To address the spectrum shortage issue, the technology of sharing the unlicensed spectrum resource has been developed for terrestrial wireless networks, e.g., the New Radio Unlicensed technology. Recently, due to the limitation of terrestrial wireless networks, unmanned aerial vehicles (UAVs) have been proposed to improve the coverage for users. Hence, the combination of the unlicensed spectrum band technology and the UAV communication can fulfill the requirements of offering 3-D coverage while improving the spectrum efficiency. In this paper, we investigate the terrestrial and UAV heterogeneous network (HetNet), where both the terrestrial base stations and aerial base stations implement the random mode selection procedure to use either the licensed or unlicensed spectrum band. Based on stochastic geometry, we develop a tractable mathematical framework to characterize the medium access probability and the overall coverage probability. The accuracy of the analytical evaluations is validated by simulations. Our results show that the incorporation of the licensed and unlicensed spectrum band by using the mode selection scheme can improve the overall network performance, compared with the performance of the 3-D HetNet operating in the licensed spectrum band only. Furthermore, mode selection of the aerial network plays the dominant role in improving the overall coverage probability, and the mode selection probability (i.e., the probability of switching to use the unlicensed spectrum band) has to be selected carefully to maximize the overall coverage probability.

INDEX TERMS Unlicensed spectrum, unmanned aerial vehicle, HetNet, poisson point process, coverage performance.

I. INTRODUCTION

With the rapid growth of applications and mobile devices in future communications, the scarcity of licensed spectrum bands has become one of the major problems for the next generation of cellular networks. To confront this issue, the 5G New Radio Unlicensed (5G NR-U) has been proposed to provide the NR-based access to the unlicensed spectrum band such that the spectrum efficiency is improved. 5G NR-U has been specified and evaluated in Release 16 by the 3rd generation partnership project [1], [2]. The coexistence of different types of devices in the unlicensed spectrum band has been widely studied [3]–[7] and most of the existing research focused on the terrestrial cellular network.

Note that the excessively large-scale deployment of conventional terrestrial networks faces many constraints. For example, for the temporary events (e.g., concerts and sports events) or the RAN congestion scenario (e.g., hotspot region in urban area during rush hours), deploying the terrestrial infrastructure can be very costly or even impractical. Under such cases, due to the advantages of versatility and high mobility, the aerial base stations (ABSs) acted by the unmanned aerial vehicle (UAV) is a suitable candidate [8]–[10]. In recent years, the heterogeneous

The associate editor coordinating the review of this manuscript and approving it for publication was Yeon-Ho Chung.

architecture by incorporating UAV communications has been considered a novel paradigm in future wireless networks. UAV communication has been widely investigated nowadays and most of the studies considered the communication in licensed spectrum bands. Due to the benefits brought by unlicensed spectrum bands, operating the UAV communications in unlicensed spectrum bands is regarded as a promising way to provide a broader coverage while enhancing the spectrum usage efficiency for future wireless communication networks.

Some works have investigated the UAV communications operating in the unlicensed spectrum band [11]–[15] recently. More specifically, the authors in [11] comprehensively reviewed the state-of-the-art resource management scenarios in LTE-Unlicensed (LTE-U) systems including the UAV systems. A game-theoretic framework for load balancing between LTE-U UAVs and the ground access points was developed in [12], where a regret-based learning dynamic duty cycle selection method for configuring the transmission gaps in LTE-U UAVs to ensure users' throughput was further proposed. In [13], licensed-assisted access technology was cooperated into the UAV communication to expand the available transmission band, where a joint trajectory design and resource allocation strategy was developed to maximize the energy efficiency. The authors in [14] proposed to introduce a cognitive UAV operating as an aerial secondary transmitter to satisfy the needs of URLLC latency and mMTC throughput by sharing the unlicensed spectrum band. The trajectory design of UAVs in a cellular network was considered in [15] to guarantee the quality of service, where the sensory data can be transmitted to the mobile devices in the unlicensed spectrum band. The aforementioned research only focused on the design in the unlicensed spectrum band. There are some other works that have also considered the design in the licensed spectrum band. Specifically, the authors in [16] studied a UAV-enabled LTE-U network for virtual reality transmission in both the licensed and unlicensed spectrum bands, and solved the resource allocation game based on the echo state networks. By utilizing the liquid state machine, this work was further extended to [17] to investigate the joint caching and resource allocation problem for a cache-enabled UAV network. In [18], the authors studied a UAV-assisted cellular network and proposed a cooperative decode-forward protocol by solving a joint resource allocation and placement problem, which aims to minimize the aggregate gap between the target rates and the throughputs of terminals. There are several other works focused on optical networks and millimeter-wave communications in the unlicensed spectrum band [19], [20].

Note that, except [16], [17], the above works considered the scenario where only the UAVs can operate in either the licensed or unlicensed spectrum band, and ignored that ground base stations (BSs) can also act as a channel competitor by implementing 5G NR-U protocol. When both UAVs and the ground BSs coexist in the licensed/unlicensed spectrum, the spectrum sharing will cause interference to each other. Consequently, the characterization of the interference and the corresponding coverage performance becomes very important, which has been ignored by the previous works.

In this work, we focus on evaluating the overall coverage performance for a 3-D HetNet constituting of terrestrial base stations (TBSs) and ABSs in the licensed and unlicensed spectrum band. This considered network can be deployed to improve the coverage for RAN congestion scenario, where the communication demand from users is massive and the spectrum resources are limited. Compared to the conventional terrestrial HetNets, the performance analysis of this complicated scenario is more challenging, since our system model involves different types of transmission links (i.e., the probabilistic channel model) and the NR-U based medium access mechanism required for the unlicensed spectrum band which will be detailed in Section II. To balance the interference in the licensed and unlicensed spectrum band, the mode selection scheme for both the TBSs and ABSs is adopted [21], i.e., both TBSs and ABSs randomly switch to use the unlicensed spectrum band with certain mode selection probability p_T and p_A, respectively.[1] By this means, the number of BSs transmitting in the licensed/unlicensed spectrum band can be adjusted. The main contributions of this work are summarized as follows:

- By using stochastic geometry, we develop a tractable mathematical framework to evaluate the medium access probability (MAP) and the coverage probability for the heterogeneous network with the random mode selection scheme. Our results show that, compared with the performance of a TBSs and ABSs HetNet where only the licensed spectrum band is used, the overall network performance can be improved by introducing the unlicensed spectrum band with appropriate mode selection.
- We come up with an approximate yet accurate analytical expression to capture the intensity of the processes of interfering TBSs and ABSs, which is an important component in determining the coverage probability in the unlicensed spectrum band. This approximation leads to the tractability of deriving the coverage probability and the accuracy of the resulted coverage performance is validated through numerical results.
- We study the impact of the mode selection probability, the intensity and the clear channel assessment (CCA) threshold of both TBSs and ABSs on the overall coverage performance. We find that the aerial network plays the dominant role in the overall coverage performance of the HetNet, while the influence from the terrestrial network is relatively slight.

The rest of this paper is organized as follows. Section II presents the system model and the considered medium access scheme. Section III describes the general formulation of the overall coverage probability, i.e., the key performance metric. The analysis for the two important factors in determining the

[1]The purpose of this work is the performance analysis for a terrestrial-UAV HetNet incorporating both the licensed and the unlicensed spectrum band. The inclusion of more sophisticated mode selection schemes (e.g., [22], [23]) is left for our future work.

overall coverage probability, i.e., the medium access probability and the conditional coverage probability, is presented in Section IV and Section V, respectively. Section VI presents the numerical and simulation results of the overall network performance. Finally, Section VII concludes the paper.

II. SYSTEM MODEL

A. SPATIAL MODEL AND MODE SELECTION SCHEME

A downlink 3-D HetNet is considered, which is constituted of TBSs, ABSs, and user equipments (UEs). The locations of TBSs and ABSs are modeled as two independent homogeneous Poisson point processes (HPPPs) on $\mathbb{R}^2$, denoted as Φ_T with intensity λ_T and Φ_A with intensity λ_A, respectively [24]. Let x_i and y_i represent the i-th TBS and i-th ABS, respectively. TBSs and UEs are located on the ground while ABSs are located in a plane with fixed height H.

The mode selection scheme [21] is adopted in this 3-D HetNet. That is to say, each TBS or ABS independently chooses to utilize either the licensed or the unlicensed spectrum band, where the microwave wireless communication is considered [1]. Let p_T and p_A denote the probability to use the unlicensed spectrum band for each TBS and ABS, respectively. The strongest average received power association strategy is considered. Depending on the type of associated BSs [25], the UE will switch to be in the licensed or the unlicensed mode. Besides, we assume that the density of UEs is far greater than the density of BSs such that each BS has at least one associated UE. Without loss of generality, we consider a typical UE located at the origin as depicted in Figure 1 and the index 0 is used to denote the typical UE as well as its serving BS.

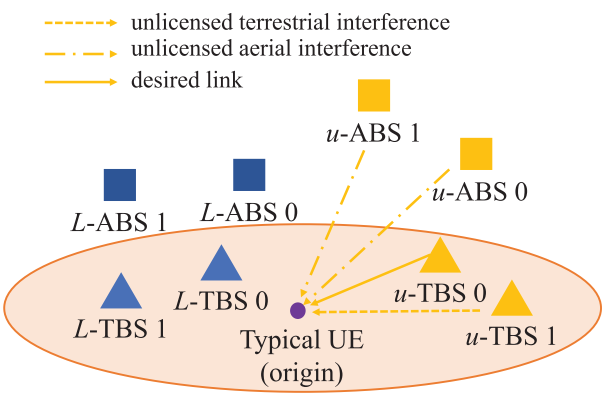

FIGURE 1. Illustration of the system model.

B. CHANNEL MODEL

In the considered network, there exist three types of links:

- air-to-air (A2A) link, i.e., the aerial link between ABSs. When using the unlicensed spectrum band, ABSs need to sense whether there is any signal exceeding the energy detection threshold on the channel or not.
- ground-to-ground (G2G) link, i.e., the terrestrial link between TBSs and UEs, and the link between unlicensed TBSs.
- air-to-ground (A2G) link, i.e., the link between ABSs and UEs, and the link between the unlicensed TBSs and unlicensed ABSs.

For the first two types of links (i.e., A2A and G2G links), we adopt the path-loss plus block fading channel model. The received power between the i-th node and the j-th node with distance d_{ij} is

$$\mathcal{PR}_{\zeta_k,\iota_k}(d_{ij}) = K_{\zeta_k}\eta_{\iota_k} g_{\iota_k,ij} d_{ij}^{-\alpha_{\iota_k}}, \tag{1}$$

where d_{ij} denotes the distance between the i-th node and the j-th node, and the symbol ζ_k is used to represent the type of occupied channel. $\zeta_k = l$ ($\zeta_k = u$) means that the licensed (unlicensed) spectrum is used. In this work, we assume that G2G link experiences the none-line-of-sight (NLoS) environment while A2A link experiences the line-of-sight (LOS) environment [26]. The symbol $\iota_k = L$ ($\iota_k = N$) indicates that the channel is in LoS (NLoS) conditions. The subscript k is used to mark the type of BSs which will be specified in Section III. $K_{\zeta_k} = (4\pi f_{\zeta_k}/c)^{-2}$ represents the free space path loss at a reference distance of 1 meter, where f_{ζ_k} is the carrier frequency and c is the speed of light. η_{ι_k} denotes the additional attenuation factor [27]. $g_{\iota_k,ij}$ denotes the block fading on the channel between the i-th node and the j-th node, which are assumed to be the same for both the licensed and the unlicensed spectrum bands [17], [28]–[30]. Specifically, $g_{N,ij}$ is assumed to be i.i.d. Nakagami-m fading with shape parameter m_N and scale parameter $\frac{1}{m_N}$, and $g_{L,ij}$ is assumed to be i.i.d. Nakagami-m fading with shape parameter m_L and scale parameter $\frac{1}{m_L}$. α_{ι_k} denotes the path-loss exponent of the channel.

As for the A2G link, we adopt the elevation angle-dependent probabilistic LoS model [27], [31], i.e., the occurrence of a LoS or NLoS channel depends on the environment parameters and the relative location between the transmitter and the receiver. The probability of being LoS transmission link is

$$p_L\left(z_{ij}\right) = \frac{1}{1 + ae^{-b\left(\arctan\left(\frac{H}{z_{ij}}\right) - a\right)}}, \tag{2}$$

where $z_{ij} = \sqrt{d_{ij}^2 - H^2}$ is the Euclidean distance between the projection of the i-th node and the j-th node on the horizontal plane. a and b are the environment parameters. Correspondingly, the probability of being NLoS transmission link is given by $p_N\left(z_{ij}\right) = 1 - p_L\left(z_{ij}\right)$.

Based on the LoS and NLoS probability, the received power on an A2G link is given by

$$\mathcal{PR}_{\zeta_k}(z_{ij}) = \begin{cases} K_{\zeta_k}\eta_L g_{L,ij} d_{ij}^{-\alpha_L}, & p_L\left(\sqrt{d_{ij}^2 - H^2}\right) \\ K_{\zeta_k}\eta_N g_{N,ij} d_{ij}^{-\alpha_N}, & p_N\left(\sqrt{d_{ij}^2 - H^2}\right). \end{cases} \tag{3}$$

TABLE 1. Summary of main symbols used in the paper.

Symbol	Definition
λ_T	Density of TBSs
λ_A	Density of ABSs
p_T	Mode selection probability for a TBS to use the unlicensed spectrum band
p_A	Mode selection probability for an ABS to use the unlicensed spectrum band
ξ_k	Symbol to indicate whether a type k BS is a TBS or an ABS ($\xi_k = T$ or A)
ζ_k	Type of the spectrum band used by a type k BS ($\zeta_k = l$ or u)
ι_k	LoS/NLoS conditions of a channel occupied by a type k BS ($\iota_k = L$ or N)
K_l	Free space path loss at a reference distance of 1 meter in the licensed spectrum band
K_u	Free space path loss at a reference distance of 1 meter in the unlicensed spectrum band
η_L	Additional attenuation factor of a link in LoS conditions
η_N	Additional attenuation factor of a link in NLoS conditions
α_L	Path-loss exponent of a link in LoS conditions
α_N	Path-loss exponent of a link in NLoS conditions
H	Height of ABSs
m_L	Nakagami-m fading parameter for a link in LoS conditions
m_N	Nakagami-m fading parameter for a link in NLoS conditions
a, b	S-curve parameters of the probability of being LoS transmission link
P_{ξ_k}	Transmit power of a type k BS
$t_{\xi_k,i}$	Random back-off period for the i-th type k BS
$b_{k,i}$	Medium access indicator assigned to the i-th type k BS
τ	SIR threshold

C. MEDIUM ACCESS SCHEME

Since the licensed and unlicensed spectrum band are involved in this work, the medium access mechanism needs to be specified for different kinds of BSs. For the case when the ground UE is associated with a BS (TBS or ABS) operating in the licensed spectrum band, the associated BS can access the channel successfully [32]. However, for the case when the ground UE is associated with a BS operating in the unlicensed spectrum band, the medium access mechanism needs to be implemented.

We consider a NR-U based medium access mechanism that generally contains two main procedures, namely the clear channel assessment procedure and the random back-off procedure [33].

- Clear channel assessment: All the transmitters operating in the unlicensed spectrum band have to sense the channel before transmitting to the UE. This procedure is conducted by sensing whether there exists any valid received signal on the channel. If a BS detects a signal whose power is higher than an energy detection threshold, the BS will take the channel as busy and continue to listen to the channel until the detected signal power on the channel is lower than the energy detection threshold. Once the BS cannot detect any valid signal exceeding the energy detection threshold, it will take the channel as idle and start the next procedure, i.e., the random back-off period. We assume that the TBS and ABS operating in the unlicensed spectrum band can perform this procedure with different energy detection thresholds. Specifically, let Δ_T and Δ_A denote this threshold for a TBS to detect the TBS's signals and the ABS's signals on the unlicensed channel, respectively. Correspondingly, the energy detection thresholds for an ABS to detect the TBS's signals and the ABS's signals on the unlicensed channel are denoted by Δ'_T and Δ'_A, respectively.
- Random back-off: If an idle channel is detected, the BS will wait for a random period to compete for the chance of transmitting signals on the channel. That is to say, a BS backing off for a shorter period can transmit its signal on the channel. This period is randomly generated from a contention window specifying the minimum and maximum waiting period for the BS. The size of the contention window determines the priority for a BS accessing the channel [34]. We denote the random back-off period for the i-th TBS and ABS by $t_{T,i}$ and $t_{A,i}$, respectively. Both $t_{T,i}$ and $t_{A,i}$ are set to be uniform random variables in the contention window [0, 1] (equivalently, the same priority for all BSs is assumed).

III. COVERAGE PROBABILITY METRIC

In this work, the overall coverage probability is adopted as the performance metric for evaluating this 3-D HetNet. This metric is defined as the average probability that the signal-to-interference (SIR) at the typical ground UE is higher than a certain threshold τ.

According to Section II, the typical UE can be either associated with an ABS or a TBS and the transmission model is different for different links. Additionally, both the TBS and ABS perform the mode selection, i.e., switch to operate in the unlicensed spectrum band with a certain probability. For such a complicated scenario, to ease the analysis, we hence classify the overall network into different types as follows.

Based on the thinning theorem in stochastic geometry [35], this HetNet is regarded as containing six types of BSs and they are

- type 1: l-TBSs. This kind of TBSs operate in the licensed spectrum band, and the links between these l-TBSs and the typical ground UE are all G2G links. Their locations follow a HPPP $\Phi_1 = \{x_{l,i}\}$ with intensity $\lambda_1 = (1 - p_T)\lambda_T$.

- type 2: u-TBSs. This kind of TBSs operate in the unlicensed spectrum band, and the links between these TBSs and the typical ground UE are all G2G links. Their locations follow a HPPP $\Phi_2 = \{x_{u,i}\}$ with intensity $\lambda_2 = p_T \lambda_T$.
- type 3: l-L-ABSs. This kind of ABSs operate in the licensed spectrum band, and the links between these ABSs and the typical ground UE are all LoS A2G links. Their locations follow an inhomogeneous Poisson point process (inHPPP) $\Phi_3 = \{y_{l,L,i}\}$ with intensity $\lambda_3\left(y_{l,L,i}\right) = (1-p_A)p_L\left(\sqrt{\|y_{l,L,i}\|^2 - H^2}\right)\lambda_A$. Note that the resulted point process is an inHPPP due to the independent thinning for the original HPPP and the fact that the intensity is not a constant but depends on the distance $\|y_{l,L,i}\|$.
- type 4: l-N-ABSs. This kind of ABSs operate in the licensed spectrum band, and the links between these ABSs and the typical ground UE are all NLoS A2G links. Their locations follow an inHPPP $\Phi_4 = \{y_{l,N,i}\}$ with intensity $\lambda_4\left(y_{l,N,i}\right) = (1-p_A)p_N\left(\sqrt{\|y_{l,N,i}\|^2 - H^2}\right)\lambda_A$.
- type 5: u-L-ABSs. This kind of ABSs operate in the unlicensed spectrum band, and the links between these ABSs and the typical ground UE are all LoS A2G links. Their locations follow an inHPPP $\Phi_5 = \{y_{u,L,i}\}$ with intensity $\lambda_5\left(y_{u,L,i}\right) = p_A p_L\left(\sqrt{\|y_{u,L,i}\|^2 - H^2}\right)\lambda_A$.
- type 6: u-N-ABSs. This kind of ABSs operate in the unlicensed spectrum band, and the links between these ABSs and the typical ground UE are all NLoS A2G links. Their locations follow an inHPPP $\Phi_6 = \{y_{u,N,i}\}$ with intensity $\lambda_6\left(y_{u,N,i}\right) = p_A p_N\left(\sqrt{\|y_{u,N,i}\|^2 - H^2}\right)\lambda_A$.

In the above setup, we use the symbol k ($k = 1, 2, \ldots, 6$) to represent the BS's type index. The symbol $\xi_k = T$ or A is used to denote whether the BS is a TBS or an ABS, and $\zeta_k = l$ or u is used to represent the type of spectrum band. In addition, $\iota_k = L$ or N is used to denote the transmission environment (LoS or NLoS).

Following the above classifications, we can mathematically express the overall coverage probability as

$$\mathbb{P}_{cov} = \sum_{k=1}^{6} \mathbb{P}_{MA}(k)\, \mathbb{P}\left(SIR_k > \tau | k\right), \tag{4}$$

where $\mathbb{P}_{MA}(k)$ is the MAP for the type k BS. It is the average probability that the typical UE is successfully associated with a type k BS and the type k BS can access the channel. $\mathbb{P}\left(SIR_k > \tau | k\right)$ is the conditional coverage probability, which is conditioned on that the typical UE is associated with a type k BS and the type k BS can access the channel.

From (4), the MAP and the conditional coverage probability determine the overall coverage probability. Their analysis is presented in the following sections.

IV. MEDIUM ACCESS ANALYSIS

Before deriving the expression of the MAP, we firstly assign a medium access indicator $b_{k,i}$ to the i-th type k BS. The indicator equals to 1 if the medium access is successful, and 0 otherwise. According to Section II-C, the medium access indicator of the type 1, 3, 4 BS is always equal to 1. Hence, the MAP for the type 1, 3, 4 BS equals to the probability that the typical ground UE is associated with a type 1, 3, 4 BS.

As for other types of BSs, since they operate in the unlicensed spectrum band, the medium access mechanism is required. The MAP for these types of BSs is the probability that the typical ground UE is associated with a type 2, 5, 6 BS and the indicator is equal to 1. The expression of this binary indicator for the i-th type k BS is given by (5), as shown at the bottom of the next page, where $\mathbf{1}(\cdot)$ is the indicator function. The point processes appeared in (5) are explained below.

To specify the component of the medium access indicator, we redivide all the other BSs operating in the unlicensed spectrum band into the following point processes from the view of the i-th type 2 BS:

- $\tilde{\Phi}_2 = \Phi_2 \backslash \{x_{u,i}\}$ with intensity λ_2 containing the type 2 BSs other than $x_{u,i}$;
- $\tilde{\Phi}_{5,2,L}$ with intensity $\lambda_5(y)\, p_L\left(\sqrt{\|y - x_{u,i}\|^2 - H^2}\right)$ containing the type 5 BSs whose links between themselves and the i-th type 2 BS are in LoS conditions;
- $\tilde{\Phi}_{5,2,N}$ with intensity $\lambda_5(y)\, p_N\left(\sqrt{\|y - x_{u,i}\|^2 - H^2}\right)$ containing the type 5 BSs whose links between themselves and the i-th type 2 BS are in NLoS conditions;
- $\tilde{\Phi}_{6,2,L}$ with intensity $\lambda_6(y)\, p_L\left(\sqrt{\|y - x_{u,i}\|^2 - H^2}\right)$ containing the type 6 BSs whose links between themselves and the i-th type 2 BS are in LoS conditions;
- $\tilde{\Phi}_{6,2,N}$ with intensity $\lambda_6(y)\, p_N\left(\sqrt{\|y - x_{u,i}\|^2 - H^2}\right)$ containing the type 6 BSs whose links between themselves and the i-th type 2 BS are in NLoS conditions.

Correspondingly, from the perspective of the i-th type $k = 5, 6$ BS, the redivided point processes are

- $\tilde{\Phi}_5 = \Phi_5 \backslash \{y_{u,\zeta_k,i}\}$ for $k = 5$ and $\tilde{\Phi}_5 = \Phi_5$ for $k = 6$;
- $\tilde{\Phi}_6 = \Phi_6$ for $k = 5$ and $\tilde{\Phi}_6 = \Phi_6 \backslash \{y_{u,\zeta_k,i}\}$ for $k = 6$;
- $\tilde{\Phi}_{2,5,L}$ with intensity $\lambda_2 p_L\left(\sqrt{\|x - y_{u,\zeta_k,i}\|^2 - H^2}\right)$ containing the type 2 BSs whose links between themselves and the i-th type 5 BS are in LoS conditions;
- $\tilde{\Phi}_{2,5,N}$ with intensity $\lambda_2 p_N\left(\sqrt{\|x - y_{u,\zeta_k,i}\|^2 - H^2}\right)$ containing the type 2 BSs whose links between themselves and the i-th type 5 BS are in NLoS conditions;
- $\tilde{\Phi}_{2,6,L}$ with intensity $\lambda_2 p_L\left(\sqrt{\|x - y_{u,\zeta_k,i}\|^2 - H^2}\right)$ containing the type 2 BSs whose links between themselves and the i-th type 6 BS are in LoS conditions;
- $\tilde{\Phi}_{2,6,N}$ with intensity $\lambda_2 p_N\left(\sqrt{\|x - y_{u,\zeta_k,i}\|^2 - H^2}\right)$ containing the type 2 BSs whose links between themselves and the i-th type 6 BS are in NLoS conditions;

Next, we present the probability density function (PDF) and the cumulative distribution function (CDF) of the distance from the typical ground UE to the associated BS in Lemma 1, which are important in determining the MAP and the conditional coverage probability.

Lemma 1: Conditioned on that the typical ground UE is associated with the type k BS, the PDF and CDF of the distance between the typical ground UE and the closest type k BS are

$$f_{R_k}(r_k)=\begin{cases} 2\pi\lambda_k r_k e^{-\pi\lambda_k r_k^2}, & k=1,2 \\ 2\pi(1-p_A)\lambda_A r_k p_{\iota_k}\left(\sqrt{r_k^2-H^2}\right) & \\ \times e^{-\int_0^{\sqrt{r_k^2-H^2}} 2\pi(1-p_A)\lambda_A z p_{\iota_k}(z)\mathrm{d}z}, & k=3,4 \\ 2\pi p_A\lambda_A r_k p_{\iota_k}\left(\sqrt{r_k^2-H^2}\right) & \\ \times e^{-\int_0^{\sqrt{r_k^2-H^2}} 2\pi p_A\lambda_A z p_{\iota_k}(z)\mathrm{d}z}, & k=5,6, \end{cases} \tag{6}$$

and

$$F_{R_k}(r_k)=\begin{cases} 1-e^{-\pi\lambda_k r_k^2}, & k=1,2 \\ 1-e^{-\int_0^{\sqrt{r_k^2-H^2}} 2\pi(1-p_A)\lambda_A z p_{\iota_k}(z)\mathrm{d}z}, & k=3,4 \\ 1-e^{-\int_0^{\sqrt{r_k^2-H^2}} 2\pi p_A\lambda_A z p_{\iota_k}(z)\mathrm{d}z}, & k=5,6, \end{cases} \tag{7}$$

respectively, where the function $p_{\iota_k}(z)$ denotes the probability of being LoS transmission link according to (2), and the subscript $\iota_k \in \{L, N\}$ denotes the LoS/NLoS conditions of a channel occupied by a type k BS.

Based on Lemma 1 and the definition of MAP, the MAPs for different types of BSs are presented in Lemmas 2-5.

Lemma 2: The medium access probability for the l-TBS (i.e., $k=1$) is given by

$$\mathbb{P}_{MA}(1)=\sum_{t=1}^{5}\int_{c_{1,t}}^{c_{1,t+1}}\phi_1(r_1)\,\mathrm{d}r_1, \tag{8}$$

$$\phi_1(r_1)\triangleq e^{-\pi\lambda_1\tilde{r}_{2,1}^2}e^{-\sum_{q=2}^{t}\int_{B\left(d_{\mathsf{h}_1(c_{1,q}),1}(r_1)\right)}\lambda_{\mathsf{h}_1(c_{1,q})}(y)\mathrm{d}y} \times f_{R_1}(r_1), \tag{9}$$

where the symbols in (8) and (9) are defined below. Note that, for $k=1,2,..,6$, the notations for these symbols share the same general formulas; hence, for notation simplicity, we present the general expressions which will be appeared in other equations, rather than defining the particular expression under $k=2$.

For $k=1,2,\ldots,6$, $c_{k,t}$ is the t-th element of the integral limit sequence C_k, where $C_k=\{0, a_k[1], a_k[2], a_k[3], a_k[4], \infty\}$ for $k=1,2$ and $C_k=\{a_k[1], a_k[2], a_k[3], a_k[4], \infty\}$ for $k=3,4,5,6$. The element in C_k, $a_k[v]$, $v=1,2,3,4$, is the v-th element of a sequence A_k sorted in the ascending order. The general expression of A_k is

$$A_k=\left\{\left(\frac{P_{\xi_k}K_{\zeta_k}\eta_{\iota_k}}{P_{\xi_3}K_{\zeta_3}\eta_{\iota_3}}\right)^{\frac{1}{\alpha_{\iota_k}}}H^{\frac{\alpha_{\iota_3}}{\alpha_{\iota_k}}},\left(\frac{P_{\xi_k}K_{\zeta_k}\eta_{\iota_k}}{P_{\xi_4}K_{\zeta_4}\eta_{\iota_4}}\right)^{\frac{1}{\alpha_{\iota_k}}}H^{\frac{\alpha_{\iota_4}}{\alpha_{\iota_k}}},\left(\frac{P_{\xi_k}K_{\zeta_k}\eta_{\iota_k}}{P_{\xi_5}K_{\zeta_5}\eta_{\iota_5}}\right)^{\frac{1}{\alpha_{\iota_k}}}H^{\frac{\alpha_{\iota_5}}{\alpha_{\iota_k}}},\left(\frac{P_{\xi_k}K_{\zeta_k}\eta_{\iota_k}}{P_{\xi_6}K_{\zeta_6}\eta_{\iota_6}}\right)^{\frac{1}{\alpha_{\iota_k}}}H^{\frac{\alpha_{\iota_6}}{\alpha_{\iota_k}}}\right\}_{\text{sorted}}. \tag{10}$$

$$b_{k,i}=\begin{cases} \prod_{x_{u,j}\in\tilde{\Phi}_2}\left(1-\mathbf{1}(t_{T,j}<t_{T,i})\mathbf{1}\left(\frac{P_T K_u\eta_N g_{N,ij}}{\|x_{u,j}-x_{u,i}\|^{\alpha_N}}\geq\Delta_T\right)\right) & \\ \times\prod_{y_{u,L,j}\in\tilde{\Phi}_{5,2,L}}\left(1-\mathbf{1}(t_{A,j}<t_{T,i})\mathbf{1}\left(\frac{P_A K_u\eta_L g_{L,ij}}{\|y_{u,L,j}-x_{u,i}\|^{\alpha_L}}\geq\Delta_A\right)\right) & \\ \times\prod_{y_{u,N,j}\in\tilde{\Phi}_{6,2,L}}\left(1-\mathbf{1}(t_{A,j}<t_{T,i})\mathbf{1}\left(\frac{P_A K_u\eta_L g_{L,ij}}{\|y_{u,N,j}-x_{u,i}\|^{\alpha_L}}\geq\Delta_A\right)\right) & \\ \times\prod_{y_{u,L,j}\in\tilde{\Phi}_{5,2,N}}\left(1-\mathbf{1}(t_{A,j}<t_{T,i})\mathbf{1}\left(\frac{P_A K_u\eta_N g_{N,ij}}{\|y_{u,L,j}-x_{u,i}\|^{\alpha_N}}\geq\Delta_A\right)\right) & \\ \times\prod_{y_{u,N,j}\in\tilde{\Phi}_{6,2,N}}\left(1-\mathbf{1}(t_{A,j}<t_{T,i})\mathbf{1}\left(\frac{P_A K_u\eta_N g_{N,ij}}{\|y_{u,N,j}-x_{u,i}\|^{\alpha_N}}\geq\Delta_A\right)\right), & k=2 \\ \prod_{y_{u,L,j}\in\tilde{\Phi}_5}\left(1-\mathbf{1}(t_{A,j}<t_{A,i})\mathbf{1}\left(\frac{P_A K_u\eta_L g_{L,ij}}{\|y_{u,L,j}-y_{u,\zeta_k,i}\|^{\alpha_L}}\geq\Delta_A'\right)\right) & \\ \times\prod_{y_{u,N,j}\in\tilde{\Phi}_6}\left(1-\mathbf{1}(t_{A,j}<t_{A,i})\mathbf{1}\left(\frac{P_A K_u\eta_L g_{L,ij}}{\|y_{u,N,j}-y_{u,\zeta_k,i}\|^{\alpha_L}}\geq\Delta_A'\right)\right) & \\ \times\prod_{x_{u,j}\in\tilde{\Phi}_{2,k,L}}\left(1-\mathbf{1}(t_{T,j}<t_{A,i})\mathbf{1}\left(\frac{P_T K_u\eta_L g_{L,ij}}{\|x_{u,j}-y_{u,\zeta_k,i}\|^{\alpha_L}}\geq\Delta_T'\right)\right) & \\ \times\prod_{x_{u,j}\in\tilde{\Phi}_{2,k,N}}\left(1-\mathbf{1}(t_{T,j}<t_{A,i})\mathbf{1}\left(\frac{P_T K_u\eta_N g_{N,ij}}{\|x_{u,j}-y_{u,\zeta_k,i}\|^{\alpha_N}}\geq\Delta_T'\right)\right), & k=5,6. \end{cases} \tag{5}$$

$\mathsf{h}_k : A_k \to \{3, 4, 5, 6\}$ denotes a mapping between the sorted integral limits and the type of ABSs. For example, if $c_{k,q} = \left(\frac{P_{\xi_k} K_{\zeta_k} \eta_{\iota_k}}{P_{\xi_{k'}} K_{\zeta_{k'}} \eta_{\iota_{k'}}}\right)^{\frac{1}{\alpha_{\iota_k}}} H^{\frac{\alpha_{\iota_{k'}}}{\alpha_{\iota_k}}}$ then $\mathsf{h}_k(c_{k,q}) = k'$. Here $\sum_{q}^{t} (\cdot) = 0$ if $t < q$.

$d_{k',k}(r_k) = \sqrt{\left(\tilde{r}_{k',k}\right)^2 - H^2}$, where the general expression of $\tilde{r}_{k',k}$ is

$$\tilde{r}_{k',k} \triangleq \left(\frac{P_{\xi_{k'}} K_{\zeta_{k'}} \eta_{\iota_{k'}}}{P_{\xi_k} K_{\zeta_k} \eta_{\iota_k}}\right)^{\frac{1}{\alpha_{\iota_{k'}}}} r_k^{\frac{\alpha_{\iota_k}}{\alpha_{\iota_{k'}}}}. \tag{11}$$

Proof: For the case of l-TBSs occupying the licensed spectrum band, since no medium access is required, its MAP is equivalent to the probability that the typical UE receives the maximum of the average received power from the closest l-TBS among all the types of BSs. Hence, we have the MAP given by

$$\begin{aligned}
&\mathbb{P}_{MA}(1) \\
&\overset{(a)}{=} E_{R_1}\left[\prod_{k'=2}^{6} \mathbb{P}\left(\frac{P_{\xi_1} K_{\zeta_1} \eta_{\iota_1}}{R_1^{\alpha_{\iota_1}}} > \frac{P_{\xi_{k'}} K_{\zeta_{k'}} \eta_{\iota_{k'}}}{R_{k'}^{\alpha_{\iota_{k'}}}}\right)\right] \\
&\overset{(b)}{=} E_{R_1}\left[\prod_{k'=2}^{6} \bar{F}_{R_{k'}}\left(\left(\frac{P_{\xi_{k'}} K_{\zeta_{k'}} \eta_{\iota_{k'}}}{P_{\xi_1} K_{\zeta_1} \eta_{\iota_1}}\right)^{\frac{1}{\alpha_{\iota_{k'}}}} R_1^{\frac{\alpha_{\iota_1}}{\alpha_{\iota_{k'}}}}\right)\right] \\
&\overset{(c)}{=} \int_0^\infty \bar{F}_{R_2}(\tilde{r}_{2,1}) \prod_{k'=3}^{6} \bar{F}_{R_{k'}}(\tilde{r}_{k',1}) f_{R_1}(r_1)\, dr_1 \\
&\overset{(d)}{=} \int_0^\infty e^{-\pi\lambda_1 \tilde{r}_{2,1}^2} \prod_{k'=3}^{6} e^{-\int_{B\left(d_{k',1}(r_1)\right)} \lambda_{k'}(y) dy} \\
&\quad \times f_{R_1}(r_1)\, dr_1,
\end{aligned} \tag{12}$$

where step (a) is due to the fact that the MAP can be interpreted as the probability that the average received power from the closest l-TBS is stronger than the average received power from the closest BS of other types, step (b) follows from the fact that the probability inside the brackets is equivalent to the complementary cumulative distribution function (CCDF) of $R_{k'}$ denoted by $\bar{F}_{R_{k'}}(\cdot)$, where the formulation of CCDF is directly related to the CDF of $R_{k'}$ and this CDF is given in Lemma 1, step (c) follows from the property that $R_{k'}$ is independent of each other, and step (d) is the substitution of CCDF's formulation. $B(r)$ denotes a disk region with radius r centered at the origin.

Note that the interval of the integral of r_1 is $[0, \infty]$. As for ABSs, due to the flying height, the interval of the integral of $r_{k'}$ is $[H, \infty]$. That is to say, the argument in the CCDF $\bar{F}_{R_{k'}}(\cdot)$ should be greater than H, i.e., $\tilde{r}_{k',1} \geq H$. This implies that $\mathbb{P}_{MA}(1)$ needs to be calculated piecewise. With proper rearrangements, we reach the general result presented in (8). ■

Lemma 3: The medium access probability for the l-L-ABS and l-N-ABS (i.e., $k = 3$ or 4) are given by

$$\mathbb{P}_{MA}(k) = \sum_{t=D+1}^{4} \int_{c_{k,t}}^{c_{k,t+1}} \phi_k(r_k)\, dr_k, \tag{13}$$

$$\begin{aligned}
\phi_k(r_k) &\triangleq e^{-\pi\lambda_1 \tilde{r}_{1,k}^2} e^{-\pi\lambda_2 \tilde{r}_{2,k}^2} \\
&\quad \times e^{-\sum_{q=1}^{D} \int_{B\left(d_{\mathsf{h}_k(c_{k,q}),k}(r_k)\right)} \lambda_{\mathsf{h}_k(c_{k,q})}(y) dy} \\
&\quad \times e^{-\sum_{q=D+2}^{t} \int_{B\left(d_{\mathsf{h}_k(c_{k,q}),k}(r_k)\right)} \lambda_{\mathsf{h}_k(c_{k,q})}(y) dy} \\
&\quad \times f_{R_k}(r_k),
\end{aligned} \tag{14}$$

where the definitions of $c_{k,t}$, h_k, and $d_{k',k}(r_k)$ are specified in Lemma 2. $D = \arg\max_D c_{k,D} < H$.

Proof: The derivation is similar to the proof of Lemma 2. Hence, we do not show the derivation for brevity. ■

Lemma 4: The medium access probability for the u-TBS is given by

$$\mathbb{P}_{MA}(2) = \sum_{t=1}^{5} \int_{c_{2,t}}^{c_{2,t+1}} \phi_2(r_2)\, dr_2, \tag{15}$$

$$\begin{aligned}
\phi_2(r_2) &\triangleq e^{-\pi\lambda_1 \tilde{r}_{1,2}^2} e^{-\sum_{q=2}^{t} \int_{B\left(d_{\mathsf{h}_2(c_{2,q}),2}(r_2)\right)} \lambda_{\mathsf{h}_2(c_{2,q})}(y) dy} \\
&\quad \times \Theta_{\xi_2}(r_2) f_{R_2}(r_2),
\end{aligned} \tag{16}$$

where the definitions of $c_{2,t}$, h_2, and $d_{k',2}(r_2)$ are specified in Lemma 2. The expressions of the function $\Theta_{\xi_2}(\cdot)$ and $Q_{\xi_k}(\cdot)$ are given in (17) and (18), respectively, as shown at the bottom of the next page, where $c_{2,t}$, h_2, and $d_{k',2}(r_2)$ are defined in Lemma 2. $\|\cdot\|$ denotes the 3-D distance from the point x to the typical ground UE and $\|x_{u,0}\| = r_2$. $\gamma(\cdot)$ is the lower incomplete gamma function and $\Gamma(\cdot)$ is the Gamma function.

Proof: See Appendix A. ■

Lemma 5: The medium access probability for the u-L-ABS and u-N-ABS (i.e., $k = 5$ or 6) are given by

$$\mathbb{P}_{MA}(k) = \sum_{t=D}^{4} \int_{c_{k,t}}^{c_{k,t+1}} \phi_k(r_k)\, dr_k, \tag{19}$$

$$\begin{aligned}
\phi_k(r_k) &\triangleq e^{-\pi\lambda_1 \tilde{r}_{1,k}^2} e^{-\pi\lambda_2 \tilde{r}_{2,k}^2} \\
&\quad \times e^{-\sum_{q=1}^{D} \int_{B\left(d_{\mathsf{h}_k(c_{k,q}),k}(r_k)\right)} \lambda_{\mathsf{h}_k(c_{k,q})}(y) dy} \\
&\quad \times e^{-\sum_{q=D+1}^{t} \int_{B\left(d_{\mathsf{h}_k(c_{k,q}),k}(r_k)\right)} \lambda_{\mathsf{h}_k(c_{k,q})}(y) dy} \\
&\quad \times \Theta_{\xi_k}(r_k) f_{R_k}(r_k),
\end{aligned} \tag{20}$$

where the definitions of $c_{k,t}$, h_k, and $d_{k',k}(r_k)$ are specified in Lemma 2, and the definition of D is specified in Lemma 3. The definition of the function $\Theta_{\xi_k}(\cdot)$ is given by

$$\begin{aligned}
&\Theta_{\xi_k}(r_k) \\
&= \frac{1 - e^{-\left(Q_{\xi_k}(5,5,\|y_{\xi_k,\zeta_k,0}\|) + \sum_{k'=5}^{6} Q_{\xi_k}(k',2,\|y_{\xi_k,\zeta_k,0}\|)\right)}}{Q_{\xi_5}(5,5,\|y_{\xi_k,\zeta_k,0}\|) + \sum_{k'=5}^{6} Q_{\xi_k}(k',2,\|y_{\xi_k,\zeta_k,0}\|)},
\end{aligned} \tag{21}$$

where $\|y_{\xi_k,\zeta_k,0}\| = r_k$.

Proof: The derivation of $\mathbb{P}_{MA}$ (5) and $\mathbb{P}_{MA}$ (6) is similar to $\mathbb{P}_{MA}$ (2); hence, we do not show its derivation for brevity. ■

V. CONDITIONAL COVERAGE PROBABILITY ANALYSIS

When the ground UE is associated with different BSs, the components of the interfering BSs are different. The formulation of SIR at a typical UE is

$$SIR_k = \begin{cases} \dfrac{P_{\xi_k} K_{\zeta_k} g_{\iota_k,0} 0 r_k^{-\alpha_{\iota_k}}}{I_{1,k} + I_{3,k} + I_{4,k}}, & k = 1, 3, 4 \\ \dfrac{b_{k,0} P_{\xi_k} K_{\zeta_k} g_{\iota_k,0} 0 r_k^{-\alpha_{\iota_k}}}{I_{2,k} + I_{5,k} + I_{6,k}}, & k = 2, 5, 6, \end{cases} \tag{22}$$

where $I_{k',k}$ denotes the aggregate interference from type k' BS and it has the form of

$$I_{k',k} = \sum_{i \in \Phi_{k'} \setminus S_{k',k}} b_{k',0} P_{\xi_{k'}} K_{\zeta_{k'}} \eta_{\iota_{k'}} g_{\iota_{k'},i0} r_{i0}^{-\alpha_{\iota_{k'}}}, \tag{23}$$

where $r_{k',i0}$ denotes the distance from the i-th interfering BS to the typical ground UE. $S_{k',k}$ represents the set of the points needed to be removed from $\Phi_{k'}$ and it is given by

$$S_{k',k} = \begin{cases} \{x_{\zeta_k,0}\}, & k = k', k = 1, 2 \\ \{y_{\zeta_k,\iota_k,0}\}, & k = k', k = 3, 4, 5, 6 \\ \emptyset, & k \neq k'. \end{cases} \tag{24}$$

A. CONDITIONAL COVERAGE PROBABILITY FOR THE LICENSED SPECTRUM SCENARIO

For the case that the typical UE is associated with a BS operating in the licensed spectrum band, the interfering BSs consists of l-TBSs, l-L-ABSs, and l-N-ABSs with the medium access indicator always being one. Their exact point processes are PPPs, as specified in Section III.

By using stochastic geometry, we can have the conditional coverage probability for the BSs operating in the licensed spectrum band given in Lemma 6.

Lemma 6: The conditional coverage probability for the l-TBS, l-L-ABS, l-N-ABS (i.e., $k = 1, 3, 4$) is given by

$$\mathbb{P}(SIR_k > \tau | k) = \int_{c_{k,1}}^{\infty} \sum_{m=0}^{m_{\iota_k}-1} \frac{s^m}{m!} (-1)^m \times \prod_{k'=1,3,4} \frac{\partial^m}{\partial s^m} \mathcal{L}_{I_{k',k}}(s) \Big|_{s = \frac{m_{\iota_k} \tau R_k^{\alpha_{\iota_k}}}{P_{\xi_k} K_{\zeta_k} \eta_{\iota_k}}} \times \tilde{f}_{R_k}(r_k)\, dr_k, \tag{25}$$

$$\Theta_{\xi_2}(r_2) = \begin{cases} \dfrac{1 - e^{-(Q_{\xi_2}(2,2,\|x_{u,0}\|))}}{Q_{\xi_2}(2, 2, \|x_{u,0}\|)}, & r_2 \le \min\{\mathsf{h}_2^{-1}(5), \mathsf{h}_2^{-1}(6)\} \\ \dfrac{1 - e^{-\left(Q_{\xi_2}(2,2,\|x_{u,0}\|) + \sum_{w=5}^{6} Q_{\xi_2}(w,5,\|x_{u,0}\|)\right)}}{Q_{\xi_2}(2, 2, \|x_{u,0}\|) + \sum_{w=5}^{6} Q_{\xi_2}(w, 5, \|x_{u,0}\|)}, & \min\{\mathsf{h}_2^{-1}(5), \mathsf{h}_2^{-1}(6)\} \le r_2 < \max\{\mathsf{h}_2^{-1}(5), \mathsf{h}_2^{-1}(6)\} \\ \dfrac{1 - e^{-\left(Q_{\xi_2}(2,2,\|x_{u,0}\|) + \sum_{k'=5}^{6}\sum_{w=5}^{6} Q_{\xi_2}(w,k',\|x_{u,0}\|)\right)}}{Q_{\xi_2}(2, 2, \|x_{u,0}\|) + \sum_{k'=5}^{6}\sum_{w=5}^{6} Q_{\xi_2}(w, k', \|x_{u,0}\|)}, & r_2 \ge \max\{\mathsf{h}_2^{-1}(5), \mathsf{h}_2^{-1}(6)\}. \end{cases} \tag{17}$$

$$Q_{\xi_k}(w, k', \|x\|) = \begin{cases} \displaystyle\int_{\mathbb{R}^2 \setminus B(\|x\|)} \left(1 - \frac{\gamma\left(m_{\iota_w}, m_{\iota_w} \frac{\Delta_T \|y-x\|^{\alpha_{\iota_w}}}{P_{\xi_{k'}} K_{\zeta_{k'}} \eta_{\iota_w}}\right)}{\Gamma(m_{\iota_w})}\right) \lambda_{k'} y dy, & \xi_k = \xi_{k'} = T \\ \displaystyle\int_{\mathbb{R}^2 \setminus B(d_{k',k}(\|x\|))} \left(1 - \frac{\gamma\left(m_{\iota_w}, m_{\iota_w} \frac{\Delta'_A \|y-x\|^{\alpha_{\iota_w}}}{P_{\xi_{k'}} K_{\zeta_{k'}} \eta_{\iota_w}}\right)}{\Gamma(m_{\iota_w})}\right) \lambda_{k'}(y)\, y dy, & \xi_k = \xi_{k'} = A \\ \displaystyle\int_{\mathbb{R}^2 \setminus B(d_{k',k}(\|x\|))} \left(1 - \frac{\gamma\left(m_{\iota_w}, m_{\iota_w} \frac{\Delta_A \|y-x\|^{\alpha_{\iota_w}}}{P_{\xi_{k'}} K_{\zeta_{k'}} \eta_{\iota_w}}\right)}{\Gamma(m_{\iota_w})}\right) \lambda_{k'}(y)\, p_{\iota_w}\left(\sqrt{\|y-x\|^2 - H^2}\right) y dy, & \xi_k = T, \xi_{k'} = A \\ \displaystyle\int_{\mathbb{R}^2 \setminus B(d_{k',k}(\|x\|))} \left(1 - \frac{\gamma\left(m_{\iota_w}, m_{\iota_w} \frac{\Delta'_T \|y-x\|^{\alpha_{\iota_w}}}{P_{\xi_{k'}} K_{\zeta_{k'}} \eta_{\iota_w}}\right)}{\Gamma(m_{\iota_w})}\right) \lambda_{k'} p_{\iota_w}\left(\sqrt{\|y-x\|^2 - H^2}\right) y dy, & \xi_k = A, \xi_{k'} = T. \end{cases} \tag{18}$$

where $\tilde{f}_{R_k}(r_k) = \phi_k(r_k)/\mathbb{P}_{MA}(k)$ is the conditional PDF of the distance from the serving BS to the typical user, given that the typical user is associated with a type k BS. $\phi_k(r_k)$ is defined in Lemmas 2-5 for different k values.

Proof: See Appendix B. ■

B. CONDITIONAL COVERAGE PROBABILITY FOR THE UNLICENSED SPECTRUM SCENARIO

For the case that the typical ground UE is associated with a BS operating in the unlicensed spectrum band, the interference comes from those unlicensed TBSs/ABSs whose medium access is also successful (i.e., the medium access indicator is equal to one). Thus the interfering processes are no longer $\Phi_k, k = 2, 5, 6$, as presented in Section III. In fact, the locations of the interfering unlicensed TBSs/ABSs follow the modified Matérn hard core process, which can be taken as a thinning process of the original PPP. But the derivation of the interference generated from such a complicated point process is highly challenging. In [33], an inHPPP with a certain intensity function is proposed to approximate this Matérn hard core process in a 2-D case. Note that such an approximation contains too many folds of integral. This can result in a complicated calculation, especially for our considered 3-D HetNet model, where the UAV is located at a certain height and the transmission scenario is much more complicated than the counterpart considered in [33]. Hence, we propose a simplified approximation of the intensity for the interfering processes in the unlicensed spectrum band. The proposed approximation results in the simpler calculation, while maintains the acceptable accuracy for the final results which will be shown in Section VI. The approximated point processes for the interfering BSs are presented in the following Proposition 1 and Corollary 1.

Proposition 1: Conditioned on that the typical UE is associated with a u-TBS $x_{u,0}$ and $b_{2,0} = 1$, the interfering BSs in the unlicensed spectrum band can be approximated by the following five inHPPPs

- $\Psi_{2,2,N}$ with intensity $\beta_{2,2,N}(x)$ containing all the interfering u-TBSs;
- $\Psi_{5,2,L}$ with intensity $\beta_{5,2,L}(y)$ containing the interfering type 5 ABSs whose links between themselves and the serving u-TBS are in LoS conditions;
- $\Psi_{5,2,N}$ with intensity $\beta_{5,2,N}(y)$ containing the interfering type 5 ABSs whose links between themselves and the serving u-TBS are in NLoS conditions;
- $\Psi_{6,2,L}$ with intensity $\beta_{6,2,L}(y)$ containing the interfering type 6 ABSs whose links between themselves and the serving u-TBS are in LoS conditions;
- $\Psi_{6,2,N}$ with intensity $\beta_{6,2,N}(y)$ containing the interfering type 6 ABSs whose links between themselves and the serving u-TBS are in NLoS conditions.

The expressions of these intensity functions are given by

$$\beta_{2,2,N}(x) = \lambda_2 N_T \left(1 - e^{-\frac{\Delta_T \|x - x_{u,0}\|^{\alpha_N}}{P_T K_u \eta_N}}\right),$$

$$\beta_{k',2,\iota}(y) = \lambda_{k'}(y) N_A p_\iota \left(\sqrt{\|x - x_{u,0}\|^2 - H^2}\right) \times \frac{\gamma\left(m_\iota, m_\iota \frac{\Delta'_T \|y - x_{u,0}\|^{\alpha_\iota}}{P_{\xi_{k'}} K_{\zeta_{k'}} \eta_\iota}\right)}{\Gamma(m_\iota)}, k' = 5, 6, \iota \in \{L, N\}, \tag{26}$$

where $N_T = \frac{1-e^{-\Upsilon_T}}{\Upsilon_T}$ and $N_A = \frac{1-e^{-\Upsilon_A}}{\Upsilon_A}$ represent the average fraction of the interfering TBSs among all of the u-TBSs and the average fraction of the interfering unlicensed ABSs among all of the ABSs operating in the unlicensed spectrum band, respectively. The symbols Υ_T and Υ_A are defined as

$$\begin{aligned}\Upsilon_T &= E_{g_{\iota_2,i0}}\left[\int_0^{\left(\frac{P_{\xi_2} K_{\zeta_2} \eta_{\iota_2} g_{\iota_2,i0}}{\Delta_T}\right)^{\frac{2}{\alpha_{\iota_2}}}} 2\pi\lambda_2 z_i \mathrm{d}z_i\right] \\ &+ E_{g_{\iota_5,i0}}\left[\int_0^{Z_{5,2}(g_{\iota_5,i0},\Delta_A)} 2\pi p_A \lambda_A p_{\iota_5}(z_i) z_i \mathrm{d}z_i\right] \\ &+ E_{g_{\iota_6,i0}}\left[\int_0^{Z_{6,2}(g_{\iota_6,i0},\Delta_A)} 2\pi p_A \lambda_A p_{\iota_6}(z_i) z_i \mathrm{d}z_i\right],\end{aligned} \tag{27}$$

$$\begin{aligned}\Upsilon_A &= E_{g_{\iota_5,i0}}\left[\int_0^{Z_{5,5}(g_{\iota_5,i0},\Delta'_A)} 2\pi p_A \lambda_A z_i \mathrm{d}z_i\right] \\ &+ E_{g_{\iota_5,i0}}\left[\int_0^{Z_{2,5}(g_{\iota_5,i0},\Delta'_T)} 2\pi\lambda_2 p_{\iota_5}(z_i) z_i \mathrm{d}z_i\right] \\ &+ E_{g_{\iota_6,i0}}\left[\int_0^{Z_{2,6}(g_{\iota_6,i0},\Delta'_T)} 2\pi\lambda_2 p_{\iota_6}(z_i) z_i \mathrm{d}z_i\right],\end{aligned} \tag{28}$$

where the function $Z_{k',k}(\cdot,\cdot)$ is

$$Z_{k',k}(g,\Delta) = \sqrt{\left(\frac{P_{\xi_{k'}} K_{\zeta_{k'}} \eta_{\iota_k} g}{\Delta}\right)^{\frac{2}{\alpha_{\iota_k}}} - H^2}. \tag{29}$$

Proof: The resulted point processes come from three procedures. Firstly, the interfering u-TBS, u-L-ABS, and u-N-ABS processes are approximated as independent thinning processes of their original point processes $\Phi_k, k = 2, 5, 6$. These three thinned point processes are denoted by Ψ_2, Ψ_5, and Ψ_6 with intensities $\lambda_2 N_T$, $\lambda_5(y) N_A$, and $\lambda_6(y) N_A$, respectively, where N_T and N_A are the average fraction of the interfering u-TBSs among all of the u-TBSs and the average fraction of the interfering ABSs among all of the unlicensed ABSs, respectively. The expressions of N_T and N_A can be obtained following the similar derivation presented in [36].

Then, by noticing that the link between a u-TBS and $x_{u,0}$ is always in NLoS conditions and the link between a u-L-ABS or u-N-ABS and $x_{u,0}$ can be in either LoS conditions or NLoS conditions, the three interfering processes Ψ_2, Ψ_5, and Ψ_6 can be further divided into five thinned PPPs, denoted by

- Ψ_2 with intensity $\lambda_2 N_T$;

- $\Psi_{5,L}$ with intensity $\lambda_5(y)N_A p_L\Big(\sqrt{\|y-x_{u,0}\|^2-H^2}\Big)$ containing ABSs in Ψ_5 whose links between themselves and the serving u-TBS are in LoS conditions;
- $\Psi_{5,N}$ with intensity $\lambda_5(y)N_A p_N\Big(\sqrt{\|y-x_{u,0}\|^2-H^2}\Big)$ containing ABSs in Ψ_5 whose links between themselves and the serving u-TBS are in NLoS conditions;
- $\Psi_{6,L}$ with intensity $\lambda_6(y)N_A p_L\Big(\sqrt{\|y-x_{u,0}\|^2-H^2}\Big)$ containing ABSs in Ψ_6 whose links between themselves and the serving u-TBS are in LoS conditions;
- $\Psi_{6,N}$ with intensity $\lambda_6(y)N_A p_N\Big(\sqrt{\|y-x_{u,0}\|^2-H^2}\Big)$ containing ABSs in Ψ_6 whose links between themselves and the serving u-TBS are in NLoS conditions.

At last, since the intensity is conditioned on $b_{2,0} = 1$, the received power at $x_{u,0}$ from the interfering u-TBSs and unlicensed ABSs should not exceed Δ_T and Δ_A, respectively. Therefore, the five approximated intensities are further multiplied by the term $\mathbb{P}\left(\frac{P_{\xi_2}K_{\zeta_2}g_{\iota_2,j0}\eta_{\iota_2}}{\|x-x_{u,0}\|^{\alpha_{\iota_2}}}<\Delta_T\right)$, $\mathbb{P}\left(\frac{P_{\xi_5}K_{\zeta_5}g_{\iota_5,j0}\eta_{\iota_5}}{\|y-x_{u,0}\|^{\alpha_{\iota_5}}}<\Delta_A\right)$, $\mathbb{P}\left(\frac{P_{\xi_5}K_{\zeta_5}g_{\iota_6,j0}\eta_{\iota_6}}{\|y-x_{u,0}\|^{\alpha_{\iota_6}}}<\Delta_A\right)$, $\mathbb{P}\left(\frac{P_{\xi_6}K_{\zeta_6}g_{\iota_5,j0}\eta_{\iota_5}}{\|y-x_{u,0}\|^{\alpha_{\iota_5}}}<\Delta_A\right)$, and $\mathbb{P}\left(\frac{P_{\xi_6}K_{\zeta_6}g_{\iota_6,j0}\eta_{\iota_6}}{\|y-x_{u,0}\|^{\alpha_{\iota_6}}}<\Delta_A\right)$, respectively. These above five terms can be obtained from the probability distribution of $g_{\iota_2,j0}$, $g_{\iota_5,j0}$, and $g_{\iota_6,j0}$. Hence, we arrive at the approximated interfering point processes presented in Proposition 1. ■

Corollary 1: Conditioned on that the typical UE is associated with a type $k = 5, 6$ BS $y_{\zeta_k,\iota_k,0}$ and $b_{k,0} = 1$, the interfering BSs in the unlicensed spectrum band can be approximated by the following four inHPPPs

- $\Psi_{2,k,L}$ with intensity $\beta_{2,k,L}(x)$ containing the interfering type 2 BSs whose links between themselves and the serving type k BS are in LoS conditions;
- $\Psi_{2,k,N}$ with intensity $\beta_{2,k,N}(x)$ containing the interfering type 2 BSs whose links between themselves and the serving type k BS are in NLoS conditions;
- $\Psi_{5,k,L}$ with intensity $\beta_{5,k,L}(y)$ containing the interfering type 5 BSs;
- $\Psi_{6,k,L}$ with intensity $\beta_{6,k,L}(y)$ containing the interfering type 6 BSs.

The specific expressions of these intensity functions are given by

$$\beta_{2,k,\iota}(x) = \lambda_2 N_T p_\iota\left(\sqrt{\|x-y_{\zeta_k,\iota_k,0}\|^2-H^2}\right)\times\frac{\gamma\left(m_\iota, m_\iota\frac{\Delta_T'\|x-y_{\zeta_k,\iota_k,0}\|^{\alpha_\iota}}{P_{\xi_2}K_{\zeta_2}\eta_\iota}\right)}{\Gamma(m_\iota)}, \tag{30}$$

$$\beta_{k',k,L}(y) = \lambda_{k'}(y)N_A\frac{\gamma\left(m_L, m_L\frac{\Delta_{\xi_{k'}}'\|y-y_{\zeta_k,\iota_k,0}\|^{\alpha_L}}{P_{\xi_{k'}}K_{\zeta_{k'}}\eta_L}\right)}{\Gamma(m_L)}, \tag{31}$$

where $k' = 5, 6$ and $\iota \in \{L, N\}$.

Proof: The derivation is similar to the proof of Proposition 1. Hence, we do not show the derivation for brevity. ■

Based on the approximated interfering processes, the expressions of SIR for type $k = 2, 5, 6$ BSs are rewritten as

$$SIR_k \approx \begin{cases}\dfrac{P_{\xi_k}K_{\zeta_k}g_{\iota_k,00}r_k^{-\alpha_{\iota_k}}}{I_{2,2,N}+I_{5,k,L}+I_{5,k,N}+I_{6,k,L}+I_{6,k,N}}, & k=2\\ \dfrac{P_{\xi_k}K_{\zeta_k}g_{\iota_k,00}r_k^{-\alpha_{\iota_k}}}{I_{2,k,L}+I_{2,k,N}+I_{5,k,L}+I_{5,k,N}}, & k=5,6,\end{cases} \tag{32}$$

where

$$I_{k',k,\iota} = \sum_{i\in\Psi_{k',k,\iota}\setminus S_{k',k}} P_{\xi_{k'}}K_{\zeta_{k'}}\eta_{\iota_{k'}}g_{i0}^{\iota_{k'}}r_{i0}^{-\alpha_{\iota_{k'}}}. \tag{33}$$

Based on the above proposition and corollary, we can derive the conditional coverage probability for the u-TBS and ABS operating in the unlicensed spectrum band, which is presented in the following corollary.

Corollary 2: The conditional SIR coverage probability of the typical ground UE when it is associated with a type 2, 5 or 6 BS is given by

$$\begin{aligned}&\mathbb{P}(SIR_2 > \tau|2)\\ &\approx \int_{c_{2,1}}^{\infty}\sum_{m=0}^{m_{\iota_2}-1}\frac{\left(\frac{m_{\iota_2}\tau r_2^{\alpha_{\iota_2}}}{P_{\xi_2}K_{\zeta_2}\eta_{\iota_2}}\right)^m}{m!}(-1)^m\mathcal{L}_{I_{2,2,N}}(s)\\ &\quad\times\prod_{k'=5,6}\prod_{\iota=L,N}\frac{\partial^m}{\partial s^m}\mathcal{L}_{I_{k',2,\iota}}(s)\Big|_{s=\frac{m_{\iota_2}\tau r_2^{\alpha_{\iota_2}}}{P_{\xi_2}K_{\zeta_2}\eta_{\iota_2}}}\\ &\quad\times\tilde{f}_{R_2}(r_2)\,\mathrm{d}r_2,\end{aligned} \tag{34}$$

$$\begin{aligned}&\mathbb{P}(SIR_k > \tau|k)\\ &\approx \int_{c_{k,1}}^{\infty}\sum_{m=0}^{m_{\iota_k}-1}\frac{\left(\frac{m_{\iota_k}\tau r_k^{\alpha_{\iota_k}}}{P_{\xi_k}K_{\zeta_k}\eta_{\iota_k}}\right)^m}{m!}(-1)^m\prod_{\iota=L,N}\mathcal{L}_{I_{2,k,\iota}}(s)\\ &\quad\times\prod_{k'=5,6}\frac{\partial^m}{\partial s^m}\mathcal{L}_{I_{k',k,L}}(s)\Big|_{s=\frac{m_{\iota_k}\tau r_k^{\alpha_{\iota_k}}}{P_{\xi_k}K_{\zeta_k}\eta_{\iota_k}}}\\ &\quad\times\tilde{f}_{R_k}(r_k)\,\mathrm{d}r_k,\quad k=5,6,\end{aligned} \tag{35}$$

where $\tilde{f}_{R_k}(r_k) = \phi_k(r_k)/\mathbb{P}_{MA}(k)$. The expression of $\phi_k(r_k)$ and $\mathbb{P}_{MA}(k)$ are presented in Lemmas 4 and 5, respectively.

Proof: The point processes of the interfering ABSs or TBSs operating in the unlicensed spectrum band are approximated as the inHPPPs with intensities specified in Proposition 1 and Corollary 1. The rest of the proof follows the same steps as given in Lemma 6. ■

C. SUMMARY

Summarily, the conditional coverage probability for different types of BSs are derived in Lemma 6 and Corollary 2, while the MAPs for different types of BSs presented in Lemmas 2-5. By substituting the conditional coverage probability and the MAP into (4), we can compute the final overall coverage probability. Note that the final overall coverage probability is composed of numerical integration and partial derivations. This is due to the complex formula of the modified sigmoid function in (2), where closed-form results are difficult to obtain, and the Nakagami-m fading model. The evaluation of the analytical results can be implemented using mathematical packages such as Mathematica.

VI. NUMERICAL EVALUATION

In this section, we first validate the analytical results of the overall coverage performance and then discuss the influences of some key system parameters on the considered HetNet. The simulation results are generated using the Monte Carlo simulations in Matlab. Unless stated otherwise, the values of the parameters are set as shown in Table 2 [37]–[39].

TABLE 2. Summary of parameter values.

Parameter	Value	Parameter	Value
P_T	40 dBm	P_A	32 dBm
f_l	4 GHz	f_u	2.4 GHz
α_L	4	α_N	2.5
η_L	1	η_N	0.2
m_L	3	λ_T, λ_A	$10^{-5}\mathrm{m}^{-2}$
a	9.6117	b	0.1581
τ	0 dB	$\Delta_T, \Delta_A, \Delta_T^{'}, \Delta_A^{'}$	-62 dBm

A. ANALYSIS VALIDATION

Figure 2 plots the overall coverage probability versus the SIR threshold with different mode selection probability. To validate the accuracy of the proposed inHPPP assumptions for the interfering BSs, we also plot the simulation results. As shown in Figure 2, the analytical results are close to the simulation results, which demonstrates the accuracy of our proposed approximations. The small gaps come from our approximated inHPPP for interfering BSs operating in the unlicensed spectrum band. Then we compare the overall coverage probabilities for the $p_T = p_A = 0$ scenario (equivalently, no TBS and ABS operate in the unlicensed spectrum band) and other scenarios. It can be observed that the overall coverage probability for the $p_T = 0.7, p_A = 0.3$ scenario is always better than that for the scenario where all BSs use the licensed spectrum band ($p_T = p_A = 0$). However, for the $p_T = 0.3, p_A = 0.7$ scenario, the overall coverage probability becomes worse when the SIR threshold τ is low, but stays better than the situation with $p_T = p_A = 0$ when the SIR threshold is high. This implies that whether the mode selection improves the overall coverage performance is related to the values of the mode selection probabilities p_T, p_A, and the SIR threshold τ. Generally, when the values of the mode selection probabilities are properly set, the incorporation of both the licensed and unlicensed spectrum band can improve the overall network coverage performance, compared with the situation where all BSs transmit in the licensed spectrum band only. The impact of the mode selection probability is investigated in the following subsections.

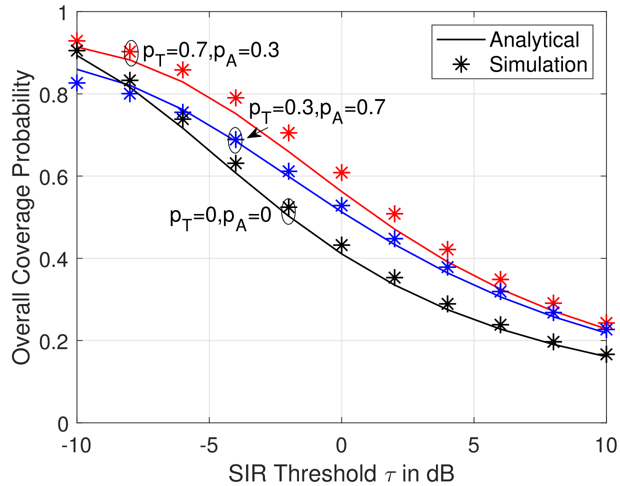

FIGURE 2. Overall coverage probability versus SIR threshold τ before and after the mode selection.

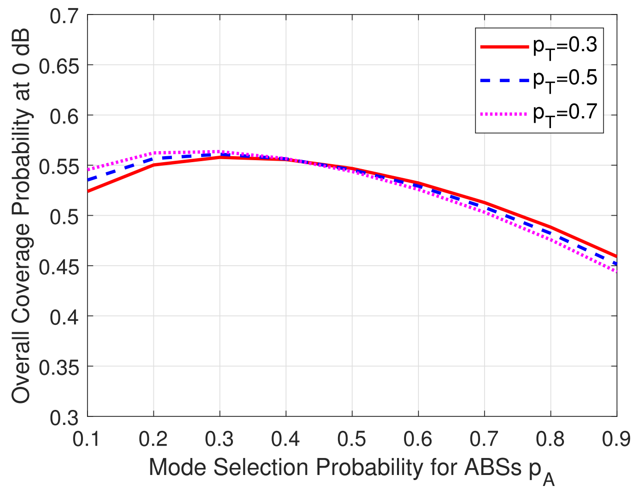

FIGURE 3. Overall coverage probability versus mode selection probability p_A with $p_T = 0.5$.

B. EFFECT OF MODE SELECTION PROBABILITY

Figure 3 plots the overall coverage probability versus the mode selection probability for ABSs p_A with a fixed $p_T = 0.5$. As illustrated in Figure 3, the overall coverage probability generally increases first but then decreases as the value of p_A increases. This phenomenon can be explained as follows. When p_A is around 0, almost all of the ABSs operate in the licensed spectrum band. Therefore the interference from these ABSs is severe, which results in the comparatively low coverage probability. While p_A is close to 1, almost all ABSs compete with each other and also with TBSs operating in the unlicensed spectrum band for the channel, which will decrease the MAP thereby deteriorating the overall coverage performance. In addition, the drop from the maximum overall coverage probability to the minimum is relatively large especially compared with that in Figure 5, which demonstrates that the aerial network is the major factor for the overall coverage performance due to the possible LoS transmissions.

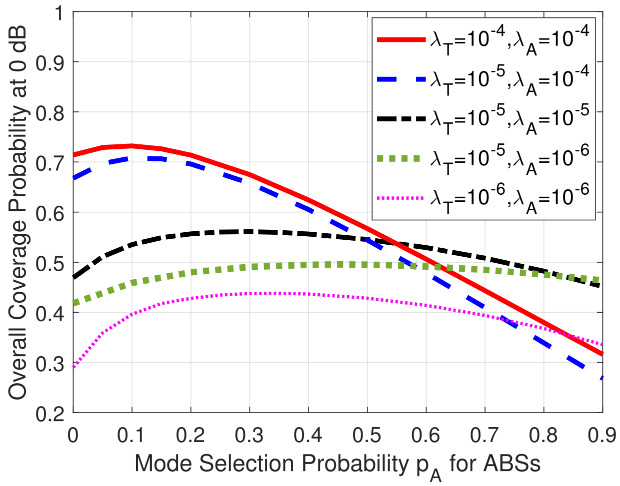

FIGURE 4. **Overall coverage probability versus p_A with different BS densities λ_T and λ_A with $p_T = 0.5$.**

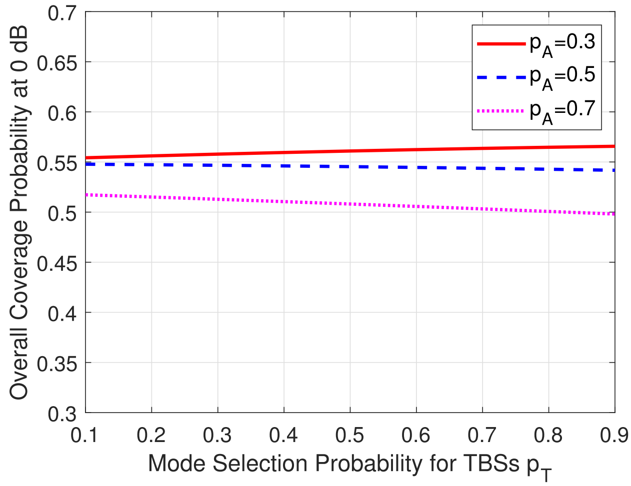

FIGURE 5. **Overall coverage probability versus mode selection probability for TBSs p_T with $p_A = 0.5$.**

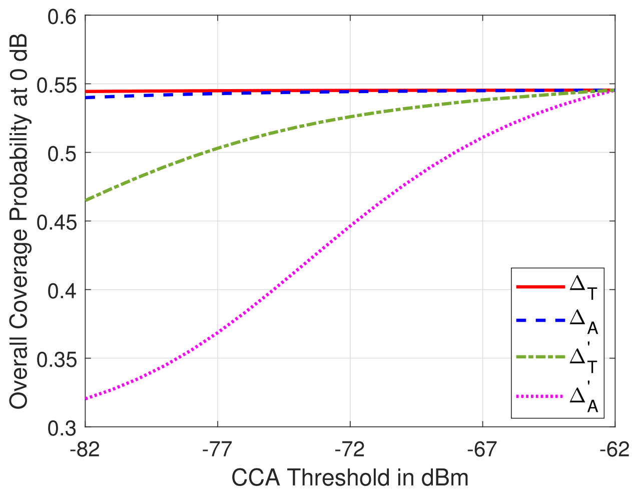

FIGURE 6. **Overall coverage probability versus CCA threshold for different types of BSs with $p_T = p_A = 0.5$.**

Figure 4 plots the overall coverage probability versus p_A with different BS densities λ_T and λ_A, under $p_T = 0.5$. It can be observed from the figure that the optimal p_A varies with BS densities. As the intensity of ABSs increases, the optimal p_A decreases, indicating that fewer ABSs using the unlicensed spectrum band are better for the overall coverage performance when ABSs are densely deployed. In contrast, as the intensity of TBSs increases, the optimal p_A increases. When TBSs become denser, the interference to the typical UE becomes severer. Since the link between the typical UE and a serving ABS is more likely to be in LoS conditions and the typical UE is likely to be covered, properly introducing more ABSs to the unlicensed spectrum band can improve the overall coverage probability. Moreover, it can be observed that as λ_T increases, the overall coverage probability improves but with a relatively small level. Comparatively, as λ_A increases, the improvement of the overall coverage probability is larger if p_A is properly set. Besides, the drop of the overall coverage probability becomes larger with the increasing of λ_A, which further indicates that the overall coverage performance is more sensitive to the change of the configuration of ABSs in the considered scenario.

Figure 5 plots the overall coverage probability versus the mode selection probability for TBSs p_T with a fixed $p_A = 0.5$. The overall coverage probability increases as p_T increases when p_A is small. However, when p_A is large, the overall coverage probability decreases with the increasing of p_T. Such kind of trends comes from the interplay of the intensity of interfering BSs, the MAP and the interference of BSs in both the licensed and unlicensed band. All in all, varying p_T influences the overall coverage probability slightly, which implies that the terrestrial network is a minor factor affecting the overall coverage performance.

C. EFFECT OF CCA THRESHOLD

Figure 6 plots the overall coverage probability versus the CCA threshold for different types of BSs when $p_T = p_A = 0.5$. Note that when one CCA value is varying, other CCA values keep fixed. According to Figure 6, the overall coverage probability increases as the CCA threshold increases. With the increasing of the CCA threshold, it is easier for BSs to detect the channel as idle and access the channel. Although more BSs accessing the channel in the unlicensed spectrum band cause the interference to some extent, whether BSs can access the channel successfully governs the overall coverage probability. Furthermore, we find that the change of the overall coverage probability when Δ_T or Δ_A increases from -82 dBm to -62 dBm is very little, while the change of the overall coverage probability when Δ'_T or Δ'_A increases from -82 dBm to -62 dBm is much larger. This further demonstrates that ABSs play the relatively dominant role when coexisted with TBSs in the unlicensed spectrum band.

VII. CONCLUSION

In this paper, we have studied the performance of the TBSs and ABSs HetNet with a mode selection scheme that allows both TBSs and ABSs to switch to use either the licensed or unlicensed spectrum band. By using stochastic geometry, a mathematical framework to characterize the overall coverage probability for this 3-D HetNet has been proposed, based on which we have examined the impact of key system parameters. Our results suggest that ABSs play the dominant role and majorly influence the overall coverage performance of the HetNet, while TBSs influence the overall coverage performance relatively slightly. Future work can consider the more complicated coexisted architectures or mode selection scheme for the terrestrial and UAV HetNet in the unlicensed spectrum band, or investigate the coverage performance when more sophisticated mode selection schemes are implemented.

APPENDIX A
PROOF OF LEMMA 4

$\mathbb{P}_{MA}(2)$ can be interpreted as the probability that the average received power from the closest u-TBS is the maximum and $b_{2,0}=1$. It can be mathematically expressed as

$$\begin{aligned}\mathbb{P}_{MA}(2) &= E_{R_2}\Bigg[\prod_{k'=1,k'\neq 2}^{6}\mathbb{P}\left(\frac{P_{\xi_2}K_{\zeta_2}\eta_{\iota_2}}{R_2^{\alpha_{\iota_2}}}>\frac{P_{\xi_{k'}}K_{\zeta_{k'}}\eta_{\iota_{k'}}}{R_{k'}^{\alpha_{\iota_{k'}}}}\right)\\ &\quad\times\mathbb{P}\left(b_{2,0}=1|r_2\right)\Bigg]\\ &=\sum_{t=1}^{5}\int_{c_{2,t}}^{c_{2,t+1}}\bar{F}_{R_1}\left(\tilde{r}_{1,2}\right)\prod_{i=3}^{6}\bar{F}_{R_{k'}}\left(\tilde{r}_{k',2}\right)\\ &\quad\times\mathbb{P}\left(b_{2,0}=1|r_2\right)f_{R_2}\left(r_2\right)\mathrm{d}r_2. \end{aligned}\tag{36}$$

$\mathbb{P}\left(b_{2,0}=1|r_2\right)$ is the conditional probability that $b_{2,0}$ is equal to one given that the distance between UE and the serving TBS is r_2.

Based on the formulation of $b_{2,0}$ shown in (5), we have this conditional probability given by (37), as shown at the bottom of the page, where $\tilde{\Phi}'_2$, $\tilde{\Phi}'_{5,2,L}$, $\tilde{\Phi}'_{6,2,L}$, $\tilde{\Phi}'_{5,2,N}$, $\tilde{\Phi}'_{6,2,N}$ represent the point processes formed by BSs with their random back-off periods smaller than $t_{T,0}$ in $\tilde{\Phi}_2$, $\tilde{\Phi}_{5,2,L}$, $\tilde{\Phi}_{6,2,L}$, $\tilde{\Phi}_{5,2,N}$, $\tilde{\Phi}_{6,2,N}$, respectively. Since $\tilde{\Phi}_2$, $\tilde{\Phi}_{5,2,L}$, $\tilde{\Phi}_{6,2,L}$, $\tilde{\Phi}_{5,2,N}$, $\tilde{\Phi}_{6,2,N}$ are PPPs according to Section IV, $\tilde{\Phi}'_2$, $\tilde{\Phi}'_{5,2,L}$, $\tilde{\Phi}'_{6,2,L}$, $\tilde{\Phi}'_{5,2,N}$, $\tilde{\Phi}'_{6,2,N}$ are still PPPs due to the independent thinning theorem. For example, the intensity of $\tilde{\Phi}'_{5,2,L}$ equals to the intensity of $\tilde{\Phi}_{5,2,L}$ multiplied by $t_{T,0}$. The step (a) comes from the CDF of $g_{\iota_2,j0}$, $g_{\iota_5,j0}$ and $g_{\iota_6,j0}$, which follows Gamma distribution. The step (b) is from the fact that $\tilde{\Phi}'_2$, $\tilde{\Phi}'_{5,2,L}$, $\tilde{\Phi}'_{6,2,L}$, $\tilde{\Phi}'_{5,2,N}$, $\tilde{\Phi}'_{6,2,N}$ are

$$\begin{aligned}&\mathbb{P}\left(b_{2,0}=1|r_2\right)\\ &=E_{t_{T,0},\tilde{\Phi}'_2,\tilde{\Phi}'_{5,2,L},\tilde{\Phi}'_{6,2,L},\tilde{\Phi}'_{5,2,N},\tilde{\Phi}'_{6,2,N}}\Bigg[\prod_{x_{u,j}\in\tilde{\Phi}'_2\setminus\{x_{u,0}\}}\left(\mathbb{P}\left(\frac{P_{\xi_2}K_{\zeta_2}\eta_{\iota_2}g_{\iota_2,j0}}{\|x_{u,j}-x_{u,0}\|^{\alpha_{\iota_2}}}\le\Delta_T\right)\right)\\ &\quad\times\prod_{y_{\zeta_5,\iota_5,j}\in\tilde{\Phi}'_{5,2,L}}\left(\mathbb{P}\left(\frac{P_{\xi_5}K_{\zeta_5}\eta_{\iota_5}g_{\iota_5,j0}}{\|y_{\zeta_5,\iota_5,j}-x_{u,0}\|^{\alpha_{\iota_5}}}\le\Delta_A\right)\right)\prod_{y_{\zeta_5,\iota_5,j}\in\tilde{\Phi}'_{5,2,N}}\left(\mathbb{P}\left(\frac{P_{\xi_5}K_{\zeta_5}\eta_{\iota_6}g_{\iota_6,j0}}{\|y_{\zeta_5,\iota_5,j}-x_{u,0}\|^{\alpha_{\iota_6}}}\le\Delta_A\right)\right)\\ &\quad\times\prod_{y_{\zeta_6,\iota_6,j}\in\tilde{\Phi}'_{6,2,L}}\left(\mathbb{P}\left(\frac{P_{\xi_6}K_{\zeta_6}\eta_{\iota_5}g_{\iota_5,j0}}{\|y_{\zeta_6,\iota_6,j}-x_{u,0}\|^{\alpha_{\iota_5}}}\le\Delta_A\right)\right)\prod_{y_{\zeta_6,\iota_6,j}\in\tilde{\Phi}'_{6,2,N}}\left(\mathbb{P}\left(\frac{P_{\xi_6}K_{\zeta_6}\eta_{\iota_6}g_{\iota_6,j0}}{\|y_{\zeta_6,\iota_6,j}-x_{u,0}\|^{\alpha_{\iota_6}}}\le\Delta_A\right)\right)\Bigg]\\ &\overset{(a)}{=}E_{t_{T,0},\tilde{\Phi}'_2,\tilde{\Phi}'_{5,2,L},\tilde{\Phi}'_{6,2,L},\tilde{\Phi}'_{5,2,N},\tilde{\Phi}'_{6,2,N}}\Bigg[\prod_{x_{u,j}\in\tilde{\Phi}'_2\setminus\{x_{u,0}\}}\frac{\gamma\left(m_{\iota_2},\frac{m_{\iota_2}\|x_{u,j}-x_{u,0}\|^{\alpha_{\iota_2}}\Delta_T}{P_{\xi_2}K_{\zeta_2}\eta_{\iota_2}}\right)}{\Gamma\left(m_{\iota_2}\right)}\\ &\quad\times\prod_{y_{\zeta_5,\iota_5,j}\in\tilde{\Phi}'_{5,2,L}}\frac{\gamma\left(m_{\iota_5},\frac{m_{\iota_5}\|y_{\zeta_5,\iota_5,j}-x_{u,0}\|^{\alpha_{\iota_5}}\Delta_A}{P_{\xi_5}K_{\zeta_5}\eta_{\iota_5}}\right)}{\Gamma\left(m_{\iota_5}\right)}\times\prod_{y_{\zeta_5,\iota_5,j}\in\tilde{\Phi}'_{5,2,N}}\frac{\gamma\left(m_{\iota_6},\frac{m_{\iota_6}\|y_{\zeta_5,\iota_5,j}-x_{u,0}\|^{\alpha_{\iota_6}}\Delta_A}{P_{\xi_5}K_{\zeta_5}\eta_{\iota_6}}\right)}{\Gamma\left(m_{\iota_6}\right)}\\ &\quad\times\prod_{y_{\zeta_6,\iota_6,j}\in\tilde{\Phi}'_{6,2,L}}\frac{\gamma\left(m_{\iota_5},\frac{m_{\iota_5}\|y_{\zeta_6,\iota_6,j}-x_{u,0}\|^{\alpha_{\iota_5}}\Delta_A}{P_{\xi_6}K_{\zeta_6}\eta_{\iota_5}}\right)}{\Gamma\left(m_{\iota_5}\right)}\times\prod_{y_{\zeta_6,\iota_6,j}\in\tilde{\Phi}'_{6,2,N}}\frac{\gamma\left(m_{\iota_6},\frac{m_{\iota_6}\|y_{\zeta_6,\iota_6,j}-x_{u,0}\|^{\alpha_{\iota_6}}\Delta_A}{P_{\xi_6}K_{\zeta_6}\eta_{\iota_6}}\right)}{\Gamma\left(m_{\iota_6}\right)}\Bigg]\\ &\overset{(b)}{=}\begin{cases}\int_0^1 e^{-t_{T,0}Q_{\xi_2}(2,2,\|x_{u,0}\|)}\mathrm{d}t_{T,0}, & r_2\le\min\{\mathrm{h}_2^{-1}(5),\mathrm{h}_2^{-1}(6)\}\\ \int_0^1 e^{-t_{T,0}\left(Q_{\xi_2}(2,2,\|x_{u,0}\|)+\sum_{j=5}^{6}Q_{\xi_2}(j,5,\|x_{u,0}\|)\right)}\mathrm{d}t_{T,0}, & \min\{\mathrm{h}_2^{-1}(5),\mathrm{h}_2^{-1}(6)\}\le r_2<\max\{\mathrm{h}_2^{-1}(5),\mathrm{h}_2^{-1}(6)\}\\ \int_0^1 e^{-t_{T,0}\left(Q_{\xi_2}(2,2,\|x_{u,0}\|)+\sum_{j=5}^{6}\sum_{i=5}^{6}Q_{\xi_2}(j,i,\|x_{u,0}\|)\right)}\mathrm{d}t_{T,0}, & r_2\ge\max\{\mathrm{h}_2^{-1}(5),\mathrm{h}_2^{-1}(6)\}.\end{cases}\end{aligned}\tag{37}$$

independent of each other and the probability generating functional (PGFL) of PPPs [40], [41].

Moreover, Note that $\mathbb{P}\left(b_{2,0}=1|r_2\right)$ is conditioned on r_2, thus $\mathbb{P}\left(b_{2,0}=1|r_2\right)$ is also a piece-wise function of r_2. By substituting $\mathbb{P}\left(b_{2,0}=1|r_2\right)$ in (37) and the CCDF $\bar{F}_{R_{k'}}\left(\tilde{r}_{k',2}\right)$ which can be obtained from Lemma 1 into (36), the result shown in Lemma 4 can be reached.

APPENDIX B
PROOF OF LEMMA 6

Conditioned on that the typical ground UE is associated with the closest type k BS, $k=1,3,4$, $\mathbb{P}\left(SIR_k>\tau|k\right)$ is

$$\begin{aligned}
&\mathbb{P}\left(SIR_k>\tau|k\right)\\
&=E_{R_k}\left[\mathbb{P}\left(g_{\iota_k,00}>\frac{\left(I_{1,k}+I_{3,k}+I_{4,k}\right)\tau R_k^{\alpha_{\iota_k}}}{P_{\xi_k}K_{\zeta_k}\eta_{\iota_k}}\right)\right]\\
&\overset{(a)}{=}\int_{c_{k,1}}^{\infty}E_{I_{1,k},I_{3,k},I_{4,k}}\left[1-\frac{\gamma\left(m_{\iota_k},\frac{m_{\iota_k}\tau\left(I_{1,k}+I_{3,k}+I_{4,k}\right)r_k^{\alpha_{\iota_k}}}{P_{\xi_k}K_{\zeta_k}\eta_{\iota_k}}\right)}{\Gamma\left(m_{\iota_k}\right)}\right]\\
&\quad\times\tilde{f}_{R_k}\left(r_k\right)\mathrm{d}r_k\\
&\overset{(b)}{=}\int_{c_{k,1}}^{\infty}\sum_{m=0}^{m_{\iota_k}-1}E_{I_{1,k},I_{3,k},I_{4,k}}\left[\left(I_{1,k}+I_{3,k}+I_{4,k}\right)^m\right.\\
&\quad\left.\times e^{-\frac{\tau m_{\iota_k}\left(I_{1,k}+I_{3,k}+I_{4,k}\right)r_k^{\alpha_{\iota_k}}}{P_{\xi_k}K_{\zeta_k}\eta_{\iota_k}}}\right]\frac{\left(\frac{\tau m_{\iota_k}r_k^{\alpha_{\iota_k}}}{P_{\xi_k}K_{\zeta_k}\eta_{\iota_k}}\right)^m}{m!}\tilde{f}_{R_k}(r_k)\mathrm{d}r_k\\
&\overset{(c)}{=}\int_{c_{k,1}}^{\infty}\sum_{m=0}^{m_{\iota_k}-1}\frac{s^m}{m!}\prod_{k'=1,3,4}E_{I_{k',k}}\left[e^{-sI_{k',k}}I_{k',k}^m\right]\Big|_{s=\frac{m_{\iota_k}\tau r_k^{\alpha_{\iota_k}}}{P_{\xi_k}K_{\zeta_k}\eta_{\iota_k}}}\\
&\quad\times\tilde{f}_{R_k}\left(r_k\right)\mathrm{d}r_k,
\end{aligned}\tag{38}$$

where the step (a) comes from the definition of the CCDF of the Gamma distribution. The step (b) comes from the definition $1-\gamma\left(m_{\iota_k},g\right)/\Gamma\left(m\right)=e^{-g}\sum_{m=0}^{m_{\iota_k}-1}g^m/m!$ and the linearity of the mathematical expectation [42]. The step (c) comes from the independency of the interference from each type of BSs. Based on the fact that $E_{I_{k',k}}\left[e^{-sI_{k',k}}I_{k',k}^m\right]=(-1)^m\frac{\partial^m}{\partial s^m}\mathcal{L}_{I_{k',k}}\left(s\right)$, the result in Lemma 6 can be reached, where $\mathcal{L}_{I_{k',k}}\left(\cdot\right)$ represents the Laplace transform of $I_{k',k}$. The expression of $\mathcal{L}_{I_{k',k}}\left(\cdot\right)$ can be derived from the PGFL of PPP [26], [43], and $\frac{\partial^m}{\partial s^m}\mathcal{L}_{I_{k',k}}\left(s\right)$ can be efficiently obtained by Faà di Bruno's rule and Bell polynomials [44].

For the conditional PDF $\tilde{f}_{R_k}\left(r_k\right)$ of r_k, we first derive the conditional CDF of r_k, which is

$$\begin{aligned}
\tilde{F}_{R_k}(r_k)=&\frac{1}{\mathbb{P}_{MA}\left(k\right)}\\
&\times E_{R_k}\left[\prod_{k'=1,k'\neq k}^{6}\mathbb{P}\left(\frac{P_{\xi_k}K_{\zeta_k}\eta_{\iota_k}}{R_k^{\alpha_{\iota_k}}}>\frac{P_{\xi_{k'}}K_{\zeta_{k'}}\eta_{\iota_{k'}}}{R_{k'}^{\alpha_{\iota_{k'}}}}\right)\right].
\end{aligned}\tag{39}$$

The rest part of the derivation is similar to the derivation presented in the proof of Lemma 2, and then the expression of the conditional CDF can be reached. Finally $\tilde{f}_{R_k}\left(r_k\right)$ can be derived via taking the first order derivative of the conditional CDF.

REFERENCES

[1] *Study on NR-Based Access to Unlicensed Spectrum (Release 16)*, document TR 38.889, 3GPP, Nov. 2018.

[2] G. Naik, J. M. Park, J. Ashdown, and W. Lehr, "Cooperative LBT design and effective capacity analysis for 5G NR ultra dense networks in unlicensed spectrum," *IEEE Access*, vol. 8, pp. 50265–50279, Apr. 2020.

[3] S. Lagen, L. Giupponi, S. Goyal, N. Patriciello, B. Bojovic, A. Demir, and M. Beluri, "New radio beam-based access to unlicensed spectrum: Design challenges and solutions," *IEEE Commun. Surveys Tuts.*, vol. 22, no. 1, pp. 8–37, 1st Quart., 2020.

[4] W. Wu, Q. Yang, R. Liu, T. Q. S. Quek, and K. S. Kwak, "Online spectrum partitioning for LTE-U and WLAN coexistence in unlicensed spectrum," *IEEE Trans. Commun.*, vol. 68, no. 1, pp. 506–520, Jan. 2020.

[5] M. Girmay, A. Shahid, V. Maglogiannis, D. Naudts, and I. Moerman, "Machine learning enabled Wi-Fi saturation sensing for fair coexistence in unlicensed spectrum," *IEEE Access*, vol. 9, pp. 42959–42974, Mar. 2021.

[6] X. Yuan, X. Qin, F. Tian, Y. T. Hou, W. Lou, S. F. Midkiff, and J. H. Reed, "Coexistence between Wi-Fi and LTE on unlicensed spectrum: A human-centric approach," *IEEE J. Sel. Areas Commun.*, vol. 35, no. 4, pp. 964–977, Apr. 2017.

[7] Y. Shi, Q. Cui, W. Ni, and Z. Fei, "Proactive dynamic channel selection based on multi-armed bandit learning for 5G NR-U," *IEEE Access*, vol. 8, pp. 196363–196374, 2020.

[8] I. Bor-Yaliniz and H. Yanikomeroglu, "The new frontier in RAN heterogeneity: Multi-tier drone-cells," *IEEE Commun. Mag.*, vol. 54, no. 11, pp. 48–55, Nov. 2016.

[9] B. Li, Z. Fei, and Y. Zhang, "UAV communications for 5G and beyond: Recent advances and future trends," *IEEE Internet Things J.*, vol. 6, no. 2, pp. 2241–2263, Apr. 2019.

[10] S. Sekander, H. Tabassum, and E. Hossain, "Multi-tier drone architecture for 5G/B5G cellular networks: Challenges, trends, and prospects," *IEEE Commun. Mag.*, vol. 56, no. 3, pp. 96–103, Mar. 2018.

[11] R. Liu, Q. Chen, G. Yu, G. Y. Li, and Z. Ding, "Resource management in LTE-U systems: Past, present, and future," *IEEE Open J. Veh. Technol.*, vol. 1, pp. 1–17, Oct. 2020.

[12] D. Athukoralage, I. Guvenc, W. Saad, and M. Bennis, "Regret based learning for UAV assisted LTE-U/WiFi public safety networks," in *Proc. IEEE Global Commun. Conf. (GLOBECOM)*, Dec. 2016, pp. 1–7.

[13] C. Xu, Q. Chen, and D. Li, "Joint trajectory design and resource allocation for energy-efficient UAV enabled eLAA network," in *Proc. IEEE Int. Conf. Commun. (ICC)*, May 2019, pp. 1–6.

[14] S. R. Sabuj, A. Ahmed, Y. Cho, K.-J. Lee, and H.-S. Jo, "Cognitive UAV-aided URLLC and mMTC services: Analyzing energy efficiency and latency," *IEEE Access*, vol. 9, pp. 5011–5027, Dec. 2021.

[15] F. Wu, H. Zhang, J. Wu, and L. Song, "Cellular UAV-to-device communications: Trajectory design and mode selection by multi-agent deep reinforcement learning," *IEEE Trans. Commun.*, vol. 68, no. 7, pp. 4175–4189, Jul. 2020.

[16] M. Chen, W. Saad, and C. Yin, "Echo state learning for wireless virtual reality resource allocation in UAV-enabled LTE-U networks," in *Proc. IEEE Int. Conf. Commun. (ICC)*, May 2018, pp. 1–6.

[17] M. Chen, W. Saad, and C. Yin, "Liquid state machine learning for resource and cache management in LTE-U unmanned aerial vehicle (UAV) networks," *IEEE Trans. Wireless Commun.*, vol. 18, no. 3, pp. 1504–1517, Mar. 2019.

[18] Y. Song, S. H. Lim, S.-W. Jeon, and S. Baek, "On cooperative achievable rates of UAV assisted cellular networks," *IEEE Trans. Veh. Technol.*, vol. 69, no. 9, pp. 9882–9895, Sep. 2020.

[19] M. T. Dabiri and S. M. Sajad Sadough, "Outage analysis of UAV-based FSO systems over log-normal turbulence channels," in *Proc. 2nd West Asian Colloq. Opt. Wireless Commun. (WACOWC)*, Apr. 2019, pp. 171–175.

[20] O. Galinina, L. Militano, S. Andreev, A. Pyattaev, K. Johnsson, A. Orsino, G. Araniti, A. Iera, M. Dohler, and Y. Koucheryavy, "Analyzing competition and cooperation dynamics of the aerial mmWave access market," *IEEE Access*, vol. 7, pp. 87192–87211, Jun. 2019.

[21] Y. Jiang, J. Guo, and Z. Fei, "Performance analysis of the coexistence of 5G NR-unlicensed and Wi-Fi with mode selection," in *Proc. IEEE/CIC Int. Conf. Commun. China (ICCC)*, Aug. 2020, pp. 953–958.

[22] A. Omri and M. O. Hasna, "A distance-based mode selection scheme for D2D-enabled networks with mobility," *IEEE Trans. Wireless Commun.*, vol. 17, no. 7, pp. 4326–4340, Jul. 2018.

[23] P. S. Bithas, K. Maliatsos, and F. Foukalas, "An SINR-aware joint mode selection, scheduling, and resource allocation scheme for D2D communications," *IEEE Trans. Veh. Technol.*, vol. 68, no. 5, pp. 4949–4963, May 2019.

[24] J. Liu, G. Wu, X. Zhang, S. Fang, and S. Li, "Modeling, analysis, and optimization of grant-free NOMA in massive MTC via stochastic geometry," *IEEE Internet Things J.*, vol. 8, no. 6, pp. 4389–4402, Mar. 2021.

[25] N. A. Elmosilhy, M. M. Elmesalawy, and A. M. Abd Elhaleem, "User association with mode selection in LWA-based multi-RAT HetNet," *IEEE Access*, vol. 7, pp. 158623–158633, Oct. 2019.

[26] M. Alzenad and H. Yanikomeroglu, "Coverage and rate analysis for vertical heterogeneous networks (VHetNets)," *IEEE Trans. Wireless Commun.*, vol. 18, no. 12, pp. 5643–5657, Dec. 2019.

[27] Y. Zeng, Q. Wu, and R. Zhang, "Accessing from the sky: A tutorial on UAV communications for 5G and beyond," *Proc. IEEE*, vol. 107, no. 12, pp. 2327–2375, Dec. 2019.

[28] R. Yin, G. Yu, A. Maaref, and G. Y. Li, "LBT-based adaptive channel access for LTE-U systems," *IEEE Trans. Wireless Commun.*, vol. 15, no. 10, pp. 6585–6597, Oct. 2016.

[29] W. Wu, Q. Yang, R. Liu, and K. S. Kwak, "Protocol design and resource allocation for LTE-U system utilizing licensed and unlicensed bands," *IEEE Access*, vol. 7, pp. 67068–67080, 2019.

[30] R. Yin, G. Yu, A. Maaref, and G. Y. Li, "A framework for co-channel interference and collision probability tradeoff in LTE licensed-assisted access networks," *IEEE Trans. Wireless Commun.*, vol. 15, no. 9, pp. 6078–6090, Sep. 2016.

[31] A. Al-Hourani, S. Kandeepan, and S. Lardner, "Optimal LAP altitude for maximum coverage," *IEEE Wireless Commun. Lett.*, vol. 3, no. 6, pp. 569–572, Dec. 2014.

[32] H. S. Dhillon, R. K. Ganti, F. Baccelli, and J. G. Andrews, "Modeling and analysis of K-tier downlink heterogeneous cellular networks," *IEEE J. Sel. Areas Commun.*, vol. 30, no. 3, pp. 550–560, Apr. 2012.

[33] Y. Li, F. Baccelli, J. G. Andrews, T. D. Novlan, and J. C. Zhang, "Modeling and analyzing the coexistence of Wi-Fi and LTE in unlicensed spectrum," *IEEE Trans. Wireless Commun.*, vol. 15, no. 9, pp. 6310–6326, Sep. 2016.

[34] J. Xiao, J. Zheng, L. Chu, and Q. Ren, "Performance modeling of LAA LBT with random backoff and a variable contention window," in *Proc. 10th Int. Conf. Wireless Commun. Signal Process. (WCSP)*, Oct. 2018, pp. 1–7.

[35] M. Haenggi, *Stochastic Geometry for Wireless Networks*. Cambridge, U.K.: Cambridge Univ. Press, 2012.

[36] H. ElSawy, E. Hossain, and S. Camorlinga, "Spectrum-efficient multichannel design for coexisting IEEE 802.15.4 networks: A stochastic geometry approach," *IEEE Trans. Mobile Comput.*, vol. 13, no. 7, pp. 1611–1624, Jul. 2014.

[37] Y. Zeng, J. Xu, and R. Zhang, "Energy minimization for wireless communication with rotary-wing UAV," *IEEE Trans. Wireless Commun.*, vol. 18, no. 4, pp. 2329–2345, Apr. 2019.

[38] X. Zhou, S. Durrani, J. Guo, and H. Yanikomeroglu, "Underlay drone cell for temporary events: Impact of drone height and aerial channel environments," *IEEE Internet Things J.*, vol. 6, no. 2, pp. 1704–1718, Apr. 2019.

[39] H. Hu, Y. Gao, J. Zhang, X. Chu, and J. Zhang, "On the performance and fairness of LTE-U and WiFi networks sharing multiple unlicensed channels," in *Proc. IEEE 30th Annu. Int. Symp. Pers., Indoor Mobile Radio Commun. (PIMRC)*, Sep. 2019, pp. 1–6.

[40] S. N. Chiu, D. Stoyan, W. S. Kendall, and J. Mecken, *Stochastic Geometry and Its Applications*. Hoboken, NJ, USA: Wiley, 2013.

[41] H. Q. Nguyen, F. Baccelli, and D. Kofman, "A stochastic geometry analysis of dense IEEE 802.11 networks," in *Proc. 26th IEEE Int. Conf. Comput. Commun. (INFOCOM)*, May 2007, pp. 1199–1207.

[42] D. Wackerly, W. Mendenhall, and R. L. Scheaffer, *Mathematical Statistics With Applications*. Belmont, CA, USA: Cengage Learning, 2007.

[43] H.-S. Jo, Y. J. Sang, P. Xia, and J. G. Andrews, "Heterogeneous cellular networks with flexible cell association: A comprehensive downlink SINR analysis," *IEEE Trans. Wireless Commun.*, vol. 11, no. 10, pp. 3484–3495, Oct. 2012.

[44] R. Tanbourgi, S. Singh, J. G. Andrews, and F. K. Jondral, "Analysis of non-coherent joint-transmission cooperation in heterogeneous cellular networks," in *Proc. IEEE Int. Conf. Commun. (ICC)*, Jun. 2014, pp. 5160–5165.

YIFAN JIANG received the B.S. degree in science in electronics engineering from Beijing Institute of Technology (BIT), China, in 2018. He is currently a master student in BIT. His research interests include heterogeneous networks and unmanned aerial vehicle communications.

ZESONG FEI (Senior Member, IEEE) received the Ph.D. degree in electronic engineering from Beijing Institute of Technology (BIT), Beijing, China, in 2004. Since September 2004, he has been with the School of Information and Electronics, BIT, where he is currently a Full Professor. He has authored or coauthored more than 120 journal articles and conference papers. His current research interests include wireless communications, channel coding, multiple access, physical layer security, joint radar and communications, and MIMO systems. He serves as an Associate Editor for IEEE ACCESS.

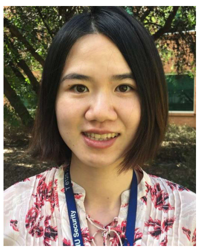

JING GUO received the joint B.Sc. degree (Hons.) in electronics and telecommunications engineering from The Australian National University, Australia, and Beijing Institute of Technology, China, in 2012, and the Ph.D. degree in telecommunications engineering from The Australian National University, in 2016. She is currently an Associate Professor with the School of Information and Electronics, Beijing Institute of Technology. Her research interests include the field of wireless communications, including heterogeneous networks, UAV networks, and the application of stochastic geometry to wireless networks.

QIMEI CUI (Senior Member, IEEE) received the B.E. and M.S. degrees in electronic engineering from Hunan University, Changsha, China, in 2000 and 2003, respectively, and the Ph.D. degree in information and communications engineering from Beijing University of Posts and Telecommunications (BUPT), Beijing, China, in 2006. She has been a Full Professor with the School of Information and Communication Engineering, BUPT, since 2014. She was a Guest Professor with the Department of Electronic Engineering, University of Notre Dame, Notre Dame, IN, USA, in 2016. Her main research interests include spectral-efficiency or energy efficiency-based transmission theory and networking technology for 4G/5G broadband wireless communications and green communications. She is a Technical Program Committee Member of several international conferences, such as the IEEE ICC, IEEE GLOBECOM, IEEE WCNC, IEEE PIMRC, IEEE/CIC ICCC, and IEEE WCSP 2013. She was a recipient of the Best Paper Award at APCC 2018, the Best Paper Award at the IEEE ISCIT 2012, the Best Paper Award at the IEEE WCNC 2014, the Honorable Mention Demo Award at the ACM MobiCom 2009, and the Young Scientist Award at the URSI GASS 2014. She is an Editor for the *Science China Information Sciences*. She is a Guest Editor for the *EURASIP Journal on Wireless Communications and Networking* and the *International Journal of Distributed Sensor Networks*.